Journal of
Synchrotron
Radiation

ISSN 1600-5775

Received 19 August 2014
Accepted 26 November 2014

Identification of the iron oxidation state and coordination geometry in iron oxide- and zeolite-based catalysts using pre-edge XAS analysis

Alexey Boubnov,[a,b] Henning Lichtenberg,[a,b] Stefan Mangold[c] and Jan-Dierk Grunwaldt[a,b]*

[a]Institute for Chemical Technology and Polymer Chemistry, Karlsruhe Institute of Technology, Kaiserstrasse 12, Karlsruhe 76131, Germany, [b]Institute of Catalysis Research and Technology, Karlsruhe Institute of Technology, Hermann-von-Helmholtz-Platz 1, Eggenstein-Leopoldshafen 76344, Germany, and [c]Synchrotron Radiation Facility ANKA, Karlsruhe Institute of Technology, Hermann-von-Helmholtz-Platz 1, Eggenstein-Leopoldshafen 76344, Germany.
*E-mail: grunwaldt@kit.edu

Analysis of the oxidation state and coordination geometry using pre-edge analysis is attractive for heterogeneous catalysis and materials science, especially for *in situ* and time-resolved studies or highly diluted systems. In the present study, focus is laid on iron-based catalysts. First a systematic investigation of the pre-edge region of the Fe *K*-edge using staurolite, $FePO_4$, FeO and α-Fe_2O_3 as reference compounds for tetrahedral Fe^{2+}, tetrahedral Fe^{3+}, octahedral Fe^{2+} and octahedral Fe^{3+}, respectively, is reported. In particular, high-resolution and conventional X-ray absorption spectra are compared, considering that in heterogeneous catalysis and material science a compromise between high-quality spectroscopic data acquisition and simultaneous analysis of functional properties is required. Results, which were obtained from reference spectra acquired with different resolution and quality, demonstrate that this analysis is also applicable to conventionally recorded pre-edge data. For this purpose, subtraction of the edge onset is preferentially carried out using an arctangent and a first-degree polynomial, independent of the resolution and quality of the data. For both standard and high-resolution data, multiplet analysis of pre-edge features has limitations due to weak transitions that cannot be identified. On the other hand, an arbitrary empirical peak fitting assists the analysis in that non-local transitions can be isolated. The analysis of the oxidation state and coordination geometry of the Fe sites using a variogram-based method is shown to be effective for standard-resolution data and leads to the same results as for high-resolution spectra. This method, validated by analysing spectra of reference compounds and their well defined mixtures, is finally applied to track structural changes in a 1% Fe/Al_2O_3 and a 0.5% Fe/BEA zeolite catalyst during reduction in 5% H_2/He. The results, hardly accessible by other techniques, show that Fe^{3+} is transformed into Fe^{2+}, while the local Fe–O coordination number of 4–5 is maintained, suggesting that the reduction involves a rearrangement of the oxygen neighbours rather than their removal. In conclusion, the variogram-based analysis of Fe *K*-edge spectra proves to be very useful in catalysis research.

Keywords: X-ray absorption spectroscopy; pre-edge peak; iron oxidation state; iron coordination geometry; heterogeneous iron catalysts; data quality; spectral resolution.

1. Introduction

Fe *K*-edge X-ray absorption spectroscopy (XAS) is a powerful tool for characterizing iron-containing materials, in particular under reaction conditions, which is important for catalysis (*e.g.* Englisch *et al.*, 1996; Grunwaldt & Clausen, 2002; Topsøe, 2003; Weckhuysen, 2003; Deutschmann & Grunwaldt, 2013, and references therein). Iron-based catalysts play a key role in several exhaust gas after-treatment systems like Fe-zeolites for selective catalytic reduction (SCR) of NO_x with NH_3 and hydrocarbons (Shelef, 1995; Marturano *et al.*, 2001; Battiston *et al.*, 2003*a*; Pirngruber *et al.*, 2004; Brandenberger *et al.*, 2008;

Høj *et al.*, 2009), CO oxidation (Wagloehner *et al.*, 2008; Royer & Duprez, 2011; Tepluchin *et al.*, 2014) and bulk processes such as Fischer–Tropsch synthesis (Dong *et al.*, 2011), ammonia synthesis (Schlögl, 2003) and ammonia decomposition (Simonsen *et al.*, 2012). XAS can be used to study catalysts *in situ* under challenging reaction conditions, since X-rays penetrate many window materials suitable for catalytic reactors specially designed for spectroscopic/catalytic experiments (Grunwaldt & Clausen, 2002; Grunwaldt *et al.*, 2004; Bare & Ressler, 2009).

It was previously shown (Westre *et al.*, 1997; Wilke *et al.*, 2001) that the pre-edge peak in Fe *K*-edge absorption spectra directly reflects the oxidation state and coordination geometry of iron in oxidic environments (Fe–O_x coordination), which allows chemical information to be retrieved from the pre-edge spectra, even if knowledge of the chemical state and geometry is limited. Typically the intensity and energy position of the pre-edge peak are graphically correlated using a scatter plot (variogram), in which the plot points corresponding to the pre-edge spectra of compounds with different oxidation states and coordination geometries have unique coordinates. A pre-edge variogram based on reference spectra of well defined oxidic iron species can thus be used as a grid for qualitative and quantitative characterization of iron species in unknown compounds.

The pre-edge peak about 10 eV below the Fe *K*-absorption edge corresponds to a $1s \rightarrow 3d$ electronic transition. For an unambiguous analysis, the main absorption edge overlapping with the pre-edge peak must be subtracted in a well defined manner, and the electronic transitions must be clearly identified, both of which requires high spectral resolution. High-resolution instruments, such as monochromator crystals with small *d*-spacing [*e.g.* Si(220) (Waychunas *et al.*, 1983; Westre *et al.*, 1997; Wilke *et al.*, 2001), Si(311) (Dräger *et al.*, 1988; Quartieri *et al.*, 2005) and Si(400) (Galoisy *et al.*, 2001)] have taken instrumental resolution close to the natural line broadening, and high-resolution fluorescence spectrometers (Battiston *et al.*, 2003*a*; Heijboer *et al.*, 2004; Pirngruber *et al.*, 2007) even beyond, giving potential to improve the acquisition and careful analysis of pre-edge data.

The variogram-based approach is simple and shows a high potential to elucidate the local environment of Fe species in complex chemical systems such as minerals, glasses and catalysts, but, to the best of our knowledge, its application is limited to studies employing high-resolution techniques (see above). Of high interest remains the extension of the variogram-based approach for pre-edge analysis to catalysis-related XAS studies using standard resolution data, especially under operating conditions. Standard XAS experiments for catalysis research are often carried out at conventional EXAFS beamlines, *e.g.* SNBL (Grunwaldt *et al.*, 2007; Doronkin *et al.*, 2014*a*) and DUBBLE (Agostini *et al.*, 2013) at ESRF, Grenoble, and ANKA XAS, Karlsruhe (Grunwaldt *et al.*, 2005), using bending-magnet radiation without beam collimation or focusing, where energy-resolution is limited by the angular divergence of the beam and by the diffraction-broadening on the monochromators, which are typically equipped with Si(111) crystals. Furthermore, a compromise between the high-quality data acquisition and catalysis-relevant measuring conditions must be found (Grunwaldt *et al.*, 2004; Bare & Ressler, 2009; Grunwaldt, 2009; Meunier, 2010). *In situ* XAS studies of highly dynamic catalytic reactions require rapid data acquisition and many catalysts contain the element of interest in low concentrations. Both effects have a direct impact on the signal-to-noise ratio. Sample inhomogeneities are also an important challenge. Dynamic changes in the catalyst structure are most clearly observable when the catalyst is a powder sample and in close contact with reactant molecules (Grunwaldt *et al.*, 2004). On the other hand, samples prepared as self-supporting wafers can provide high-quality spectra, but diffusion limitations limit the relevance of these studies for catalytic reactions.

The objective of this work is to investigate whether procedures described in literature to extract chemical information from pre-edge data acquired with high resolution can also be used on catalysts under challenging reaction conditions at conventional XAS beamlines. For this purpose, the effect of the spectral resolution and data quality (in terms of energy increments) is systematically studied at different steps of the pre-edge analysis. Firstly, the edge subtraction from XANES spectra of a reference compound acquired with different resolution and quality is tested with several model functions. It is shown that resolution and quality of the measured spectra are less critical than the choice of the model function. After successful edge subtraction, the pre-edge spectra are deconvoluted, which is useful for arbitrarily separating local from non-local transitions (*e.g.* in α-Fe_2O_3) and works for both high and standard resolution, but is less suitable for multiplet analysis, since not all transitions can be identified. The subsequent variogram-based chemical analysis is verified using binary mixtures of reference compounds and a library of compounds containing pure and mixed Fe species, showing that the analysis of standard-resolution pre-edge spectra leads to the same results as those obtained from high-resolution spectra. Finally, structural changes in a 1% Fe/Al_2O_3 catalyst and a 0.5% Fe/BEA zeolite catalyst during reduction in 5% and 20% H_2/He gas mixtures, respectively, are studied to verify the applicability of pre-edge spectroscopy for chemical analysis in the field of catalysis research.

2. Experimental

2.1. Fe *K*-edge XANES measurements

XAFS measurements at the Fe *K*-edge were carried out at the ANKA synchrotron light source (Karlsruhe, Germany) at the XAS beamline using bending-magnet radiation and a double-crystal monochromator equipped with Si(111) crystals. The ANKA storage ring was operated at an electron energy of 2.5 GeV and currents of 80–160 mA. At 100 mA ring current the XAS beamline provides an unfocused beam with a flux of *ca* 5×10^9 photons s^{-1} mm^{-2} at the Fe *K*-edge. The monochromator was detuned to 70% of the maximum intensity for rejection of higher harmonics. For X-ray absorption

measurements in transmission mode, the incoming and transmitted monochromatic intensity was measured using ionization chambers (Oxford) filled with appropriate mixtures of Ar, N_2 and He to achieve absorption of 15% in the first, 40% in the second and 60% in the third ionization chamber at 7500 eV, close to the centre of an Fe *K*-edge EXAFS scan interval. The sample was placed between the first and second ionization chamber, and a Fe foil between the second and the third. The absorption coefficient was calculated according to the Lambert–Beer law. Measurements in fluorescence mode were carried out using an energy-dispersive five-element solid-state Ge detector (Canberra, Fe $K\alpha$ emission lines, line width of 300 eV, peaking time of 500 ns).

The instrumental resolution and the beam profile at the sample position are defined by a system of mechanical slits: for standard resolution measurements, the vertical beam size is limited to 1.2 mm in front of the monochromator and 1 mm downstream. Under these conditions, the instrumental line broadening is approximately 1.2 eV, determined by radiography (Mangold *et al.*, 2013). The monochromator was operated in continuous scanning mode with data point acquisition in 0.5 eV increments. These energy increments are sufficient to account for the shape of the spectral features, which are influenced by the line broadening due to instrumental resolution and the core-hole lifetime.

For measurements with higher resolution the vertical beam size was set to 0.3 mm in front of the monochromator and 0.15 mm downstream to decrease the beam divergence. This reduced the instrumental line width to approximately 0.8 eV. These high-resolution spectra were acquired in a step-scanning mode in 0.25 eV energy increments. The horizontal beam dimension was adjusted to the size of the sample: for measuring pellet samples, it was set to 8 mm, and for *in situ* experiments it was adjusted to the smaller sample area with slits downstream of the monochromator.

Higher-resolution *in situ* measurements were conducted at the MAX-lab synchrotron radiation facility (Lund, Sweden) at the I811 beamline, using wiggler radiation and beam collimation, thus avoiding the effect of instrumental broadening due to angular divergence. The beam was focused at the sample to a spot of 0.5 mm × 0.5 mm with an intensity of 10^{11}–10^{12} photons s^{-1}. The instrumental line width was *ca* 0.7 eV. The photon energy was scanned in continuous mode using a double-crystal monochromator equipped with Si(111) crystals, recording data points in 0.1 eV increments.

2.2. HERFD-XANES measurements

XANES measurements in high-energy-resolution fluorescence-detection (HERFD) mode were performed at the ID26 undulator beamline at the European Synchrotron Radiation Facility (ESRF, Grenoble, France) using a double-crystal monochromator equipped with Si(111) crystals (collimated incident beam) and a spectrometer equipped with spherically bent Ge(620) analyser crystals (r = 1 m) in Rowland geometry (Glatzel *et al.*, 2009; Atkins *et al.*, 2013). The absorption coefficient was measured in fluorescence mode (detector window set to the maximum of the Fe $K\beta_{1,3}$ emission line, incident beam intensity measured with a photodiode). XANES spectra were acquired by scanning the monochromator in continuous mode and integrating the measured intensity over 0.05 eV energy increments. The instrumental resolution at 7113 eV was 1.4 eV, determined as the energy line width of an elastically scattered beam, which accounts for the line broadening due to both the monochromator and the spectrometer. This instrumental line width is well below the core-hole line width of the Fe $K\beta_{1,3}$ emission line (*ca* 4.5 eV), allowing a highly specific detection of this electronic transition as a secondary process of the X-ray absorption.

2.3. Fe-bearing reference compounds

Reference compounds, minerals and oxides representing different chemical states of iron, are presented in Table 1. The minerals olivine, siderite, aegirine, ceylonite and bronzite were received from Federal State Unitary Enterprise 'All-Russian Research Institute of Mineral Resources' (FGUP 'VIMS', Moscow, Russia) and Moscow Geological Prospecting Institute, Russian State Geological Prospecting University (MGRI-RSGPU, Moscow, Russia). Staurolite, magnetite and sanidine were provided by the Institute of Applied Geosciences (KIT, Karlsruhe, Germany). The minerals have been analysed by the groups. Additionally, high-purity iron nitrate, rodolicoite, wustite, maghemite and iron phthalocyanine were purchased from the indicated manufacturers. Previously characterized haematite, amorphous hydrated iron phosphate, iron (III) acetylacetonate and iron (II) oxalate were kindly provided by the corresponding author. The samples were prepared as pellets (pressed with cellulose). The Fe content was adjusted to an absorption length resulting in an edge jump of between 0.3 and 0.9. Six mechanical binary mixtures of the compounds staurolite, FeO, $FePO_4$ and α-Fe_2O_3 were prepared with Fe stoichiometric ratios close to 50:50.

2.4. *In situ* XANES and H_2-TPR of Fe/Al_2O_3 and Fe/BEA

The Fe/Al_2O_3 catalyst was prepared by incipient wetness impregnation of γ-Al_2O_3 with an aqueous solution of iron nitrate followed by drying and calcination at 600°C. The resulting Fe content was 1% by weight. The Fe/BEA catalyst was prepared by incipient wetness impregnation of the BEA zeolite to obtain a Fe-loading of 0.5% by weight (Høj *et al.*, 2009). For *in situ* TPR measurements, a sieve fraction of 100–200 µm catalyst powder was exposed to a flow of 5% H_2 in balance He in a quartz capillary micro-reactor [*cf.* setup of Grunwaldt *et al.* (2005), Høj *et al.* (2009) and Klukowski *et al.* (2009)]. XANES spectra of the Fe/Al_2O_3 catalyst were acquired with standard resolution (at ANKA XAS) in fluorescence mode during continuous scanning of the monochromator (*ca* 4 min per spectrum). XANES spectra of the 0.5% Fe/BEA catalyst were acquired with high resolution in fluorescence mode (at MAX-lab, I811). Acquisition of one spectrum took *ca* 5 min.

Table 1
Chemical composition of the reference compounds used in this study and the mode of measurement used for acquiring the XANES spectra.

The list is sorted according to valence (Fe^{2+} and Fe^{3+}) and coordination symmetry of the Fe ions (tetrahedral T_d, octahedral O_h, square planar and mixed).

	Samples	Fe state	Measurement modes
Fe^{3+} O_h	Haematite α-Fe_2O_3		Transmission (standard and high resolution)
	$FePO_4{\cdot}xH_2O$		Transmission (standard resolution)
	Fe(III)acac		Transmission (standard resolution)
	$Fe(NO_3)_3{\cdot}9H_2O$ (Prolabo)		Transmission (standard resolution)
	Aegirine $NaFeSi_2O_6$ (Russia)		Transmission (standard resolution)
Fe^{3+} T_d	Rodolicoite $FePO_4$ (Merck)		Transmission (standard and high resolution)
	Sanidine $(K,Na)(Si,Al,Fe)_4O_8$ (Eifel, Germany) (Ginibre *et al.*, 2004)		Fluorescence (standard resolution)
Fe^{2+} O_h	Wustite FeO (Aldrich)		Transmission (standard and high resolution)
	Fe(II)oxalate		Transmission (standard resolution)
	Siderite $FeCO_3$ (Russia)		Transmission (standard resolution)
	Olivine $(Mg,Fe)_2SiO_4$ (Sakha Rep, 'Mir' diamond mine)		Transmission (standard resolution)
	Bronzite $(Mg,Fe)_2Si_2O_6$ (Polar Ural, Russia)		Transmission (standard resolution)
Fe^{2+} T_d	Staurolite $Fe_2Al_9O_6(SiO_4)_4(O,OH)_2$		Transmission (standard and high resolution), HERFD
	Ceylonite $(Mg,Fe)Al_2O_4$ (Russia)		Transmission (standard resolution)
Others	Maghemite γ-Fe_2O_3 (Alfa Aesar)	Fe^{+3}, T_d and O_h	Transmission (standard resolution)
	Magnetite Fe_3O_4	Fe^{+2}, Fe^{+3}, T_d and O_h	Transmission (standard resolution)
	Fe(II) phthalocyanine (Alfa Aesar)	Fe^{+2}, square planar	Transmission (standard resolution)

2.5. XANES data processing

The spectra were analysed using the *Athena* interface of the *IFEFFIT* software package (Newville, 2001). All spectra were calibrated to the first inflection point in a simultaneously measured Fe foil spectrum set at 7112.0 eV. Note that this value varies from study to study, *e.g.* 7111.08 eV (Wilke *et al.*, 2001) and 7111.2 eV (Westre *et al.*, 1997). Subsequently, the XAS spectra were normalized using a first-degree polynomial fitted below the edge and a second-degree polynomial fitted above the edge. The stoichiometric ratios of the Fe species in the binary mixtures of reference compounds measured in transmission mode with high resolution were determined using linear combination analysis (LCA). To generate spectra of mixtures, normalized XANES spectra of reference compounds measured with standard resolution were merged in the required ratios.

Reduction of iron during the TPR experiments was probed by LCA of the *in situ* recorded XANES spectra, using the first and last spectrum of the TPR series as reference spectra. LCA was carried out in the energy range between 7102 eV (below the pre-edge region) and 7155 eV (first isosbestic point above the first maximum beyond the edge).

2.6. Pre-edge peak analysis

The pre-edge peaks of the normalized XANES spectra were analysed using MATLAB codes based on procedures described in literature (Roe *et al.*, 1984; Galoisy *et al.*, 2001; Wilke *et al.*, 2001, 2005; Quartieri *et al.*, 2005). The absorption-edge onset was modelled by fitting the energy regions below and above the pre-edge feature (see §3.1) and subsequently subtracted to extract the pre-edge peak. Four methods for extraction of the pre-edge peak were initially examined: interpolation by a cubic spline, fitting with an arctangent, an inclined arctangent (arctangent with a first-degree polynomial) and two Gaussian functions with a shared centre. One of these Gaussian functions was broad and flat to account for the increase in absorption before the pre-edge region; the other was narrow and intense to account for the edge onset. The inclined arctangent was used in all successive analysis.

The spline interpolation with not-a-knot end conditions was applied to the XANES data. When the model functions were fitted to the XANES spectra, all parameters were allowed to float within limits set far from the target values; the function converged to the data points with standard deviations of the order of 1% of the normalized pre-edge peak height (*ca* 0.1). The values of the model function should preferentially not exceed the values of the experimental data above the edge (*e.g.* the arctangent should tend to a value below 1). A crucial step was the individual selection of fitting intervals for each spectrum. The fitting range in the edge onset area was extended as far as it could be modelled with the appropriate functions.

As a further step, electronic transitions in the extracted pre-edge features (in the following referred to as pre-edge spectra) were fitted with peak functions (Wilke *et al.*, 2001). The MATLAB procedure for this step automatically fitted one to five pseudo-Voigt functions with variable full width at half-maximum (FWHM) and Gaussian fraction. The first fit of the pre-edge feature was carried out with a single pseudo-Voigt peak function. The starting guess values for the further four fits (two to five peaks) were obtained from the results of the first fit. The starting situation for a two-peak fit was the use of two peaks of half the area of the single peak separated by half

the FWHM of the single peak. Accordingly, for a three-peak fit, three peaks of a third of the area of the single peak separated by one-third of the FHWM of the single peak were used as initial guesses, *etc*. The FWHM and Gaussian fraction were constrained to be shared by all peaks within one fit, but their values were not fixed. Further analysis of the pre-edge spectra with respect to the oxidation state and local geometry of Fe was carried out graphically according to Wilke *et al.* (2001) by correlating the integrated intensity and the centroid position (*i.e.* the area-based average energy position) of the pre-edge peak.

Similar curve-fitting procedures are used in X-ray absorption data processing packages [*SixPACK* (Webb, 2005) and *Athena* (Ravel & Newville, 2005), both based on *IFEFFIT*], but are not easy to change or adapt for users. For example, the application of shared fitting parameters for several model functions and automatic assignment of the starting guesses as described above are limited. Alternatively, commercial software such as *PeakFit* (Systat Software Inc.) can be used for pre-edge analysis (Quartieri *et al.*, 2005), but with limited access to several different fits. On the contrary, the MATLAB-based procedure used in this study allows examination of fits with a different number of peaks and selection of the most suitable one. The optimum number of pseudo-Voigt peaks for modelling the pre-edge feature was chosen based on the quality of fit, preliminary knowledge of the expected number of electronic transitions as well as the peak width and a Gaussian fraction consistent with the instrumental resolution. Moreover, several possibilities, such as wider peaks accounting for overlapping transitions, can be taken into account. Multiple data sets can be analysed in parallel, starting parameters can be stored and manipulated in input text files, and output data files are generated after each analysis.

3. Results and discussion

3.1. Pre-edge extraction functions and effect of resolution

To find the most suitable model functions for pre-edge extraction in an empirical way, several functions were tested for later analysis of iron-based catalysts. For modelling the absorption edge onset, steeply increasing functions have been used in several studies, such as a second-degree polynomial (Bajt *et al.*, 1994), arctangent (Galoisy *et al.*, 2001; Quartieri *et al.*, 2005), arctangent with a first-degree polynomial (Roe *et al.*, 1984), damped harmonic oscillator function (Cottrell *et al.*, 2009) or several peak functions (Westre *et al.*, 1997; Farges *et al.*, 2004; Farges, 2005; Wilke *et al.*, 2005). Therefore we investigated here how different functions (inclined arctangent, arctangent, two Gaussians and the cubic spline) modelled the background of the XANES spectra of staurolite, acquired with different energy resolution and corresponding energy increments: transmission-mode with standard resolution (0.5 eV and 1 eV increments) and high resolution (0.25 eV increments), and, for comparison, HERFD-XANES (0.05 eV increments).

The HERFD-XANES spectrum of staurolite in Fig. 1(*a*) shows a pre-edge feature well separated from the edge onset, which is due to the specific detection of the Fe $K\beta_{1,3}$ fluorescence line with high resolution, excluding all other transitions. All model functions subtract the small contribution of the edge onset from the pre-edge feature in a similar manner (Fig. 1*b*) and with high quality (low residuals and standard deviation σ). The transmission-mode XANES spectrum of staurolite measured with high resolution (Fig. 1*c*) differs from the HERFD-XANES spectrum with a strong background consisting of the edge onset tail, comparing Figs. 1(*b*) and 1(*d*). This is caused by a continuum of electronic transitions resulting from photoabsorption, which all contribute to the transmission spectrum. Like in the HERFD-XANES spectrum measured at ID26 (ESRF), the double feature in the pre-edge region can be identified in the transmission-mode spectrum measured at ANKA XAS, due to the enhanced energy-resolution of this beamline with reduced slit widths.

For subtraction of the pre-edge peak from the edge onset, the functions modelled the edge onset in the high-resolution transmission spectrum up to about 0.5 normalized absorption (Fig. 1*c*), whereas a portion up to only *ca* 0.1 normalized absorption was necessary in the HERFD-XANES data (Fig. 1*a*). The standard deviations (σ) in the regions below and above the pre-edge peak were an order of magnitude higher in the high-resolution transmission XANES than in the HERFD-XANES, shown along with the extracted pre-edge spectra in Figs. 1(*a*) and 1(*c*), magnified by factors of 100 and 10, respectively. The best-converging functions for modelling the edge onset in the transmission-mode spectra acquired with high resolution [Fig. 1(*c*) and zoom in Fig. 1(*d*)] were the simple and the inclined arctangent function. The inclined arctangent can correct any constant gradient component at the expense of including the inclination slope as one extra parameter.

The edge onset could also be modelled by two Gaussians, but with a larger standard deviation. Only the low-energy side of this peak function was used in the fit. This feature is characterized by two slopes joined by a smooth kink, which can indeed be a good model for the shape of the transmission XANES spectrum in Fig. 1(*c*). On the other hand, in the pre-edge region this function is more rigid than the arctangent functions and tends to 'cut' through the pre-edge feature [clearly visible in Fig. 1(*d*)], truncating it in intensity and distorting the width and shape of the peak. It is possible that this effect can be eliminated by letting the two Gaussian peaks centre at individual positions (Wilke *et al.*, 2005).

Different for cubic spline interpolation is that the spline passes exactly through the points below and above the pre-edge region, leaving no residuals. Interpolation of points below and above the pre-edge feature using a cubic spline has been reported previously (Wilke *et al.*, 2001; Battiston *et al.*, 2003*a*,*b*). Cubic spline interpolation is well suited for high-quality data but very sensitive to noise, as slight displacement of data points can, however, lead to unreasonable deviations. Even pre-edge data measured with standard resolution can be extracted using cubic splines, but require a low noise level and

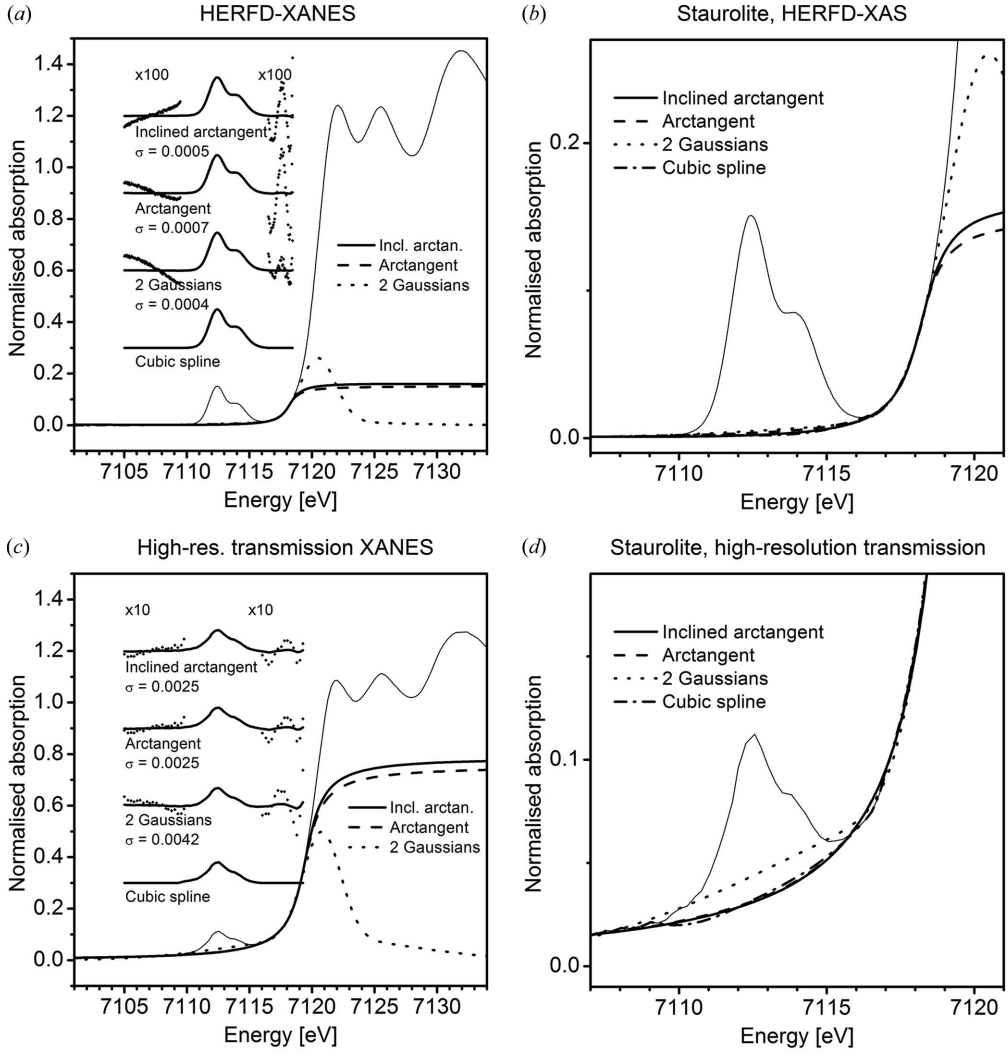

Figure 1
XANES spectra of staurolite and pre-edge extraction models for HERFD-XANES data recorded in 0.05 eV increments (*a*) and high-resolution transmission-mode XANES data recorded in 0.25 eV increments (*c*). The functions for modelling the edge onset, *i.e.* the inclined arctangent, arctangent, two Gaussian functions and cubic spline, are displayed with the XANES spectra they are applied to. The resulting extracted pre-edge peaks are shown offset for clarity. The fitting residuals are magnified by a factor of 100 (HERFD) and 10 (high-resolution transmission) to show the misfit and the standard deviation (σ) is given. Details in the pre-edge region of plots (*a*) and (*c*) are shown in plots (*b*) and (*d*), respectively.

dense data points (Berry *et al.*, 2003). To maintain a stable trajectory of the spline across this rather large gap in the present work, an additional knot was manually included in the pre-edge region. However, this is not acceptable for a reproducible and objective approach and interpolation by cubic splines was not pursued further in this work.

In the case of the XANES spectrum measured with standard resolution in 0.5 eV energy increments [Fig. 2(*a*), zoom in Fig. 2(*b*)], the fit quality followed a similar trend as for the high-resolution transmission spectrum: the inclined arctangent and the arctangent were superior. The standard-resolution spectrum measured in 1 eV energy increments [Fig. 2(*c*), zoom in Fig. 2(*d*)] was generated by removing every second data point from the spectrum acquired in 0.5 eV increments. The inclined arctangent was superior over the simple arctangent function, as in the case of better data quality. To address the challenge of data quality in terms of the data point sampling density, the transmission-mode XANES spectra shown in Figs. 1(*c*) and Figs. 2(*a*) and 2(*c*) were recorded with varying increments (0.25, 0.5 and 1 eV). However, the background subtraction by the three functions remains the same and does not depend on the data point density. From this observation it can be concluded that a high data point density has hardly any influence on the quality of the background subtraction. On the other hand, the data point density should be sufficient for resolving the spectral features, otherwise spectral information is lost, as for example shown in Fig. 2(*c*) (1 eV energy increments). The inclined arctangent and the arctangent function turned out to be well suited candidates for subtraction of the main edge onset contribution in transmission-mode XANES data acquired with standard and high resolution. As the slope in the inclined arctangent provides additional adjustments for improving the quality of fitting in the background-subtracting step, this function was used in the following sections.

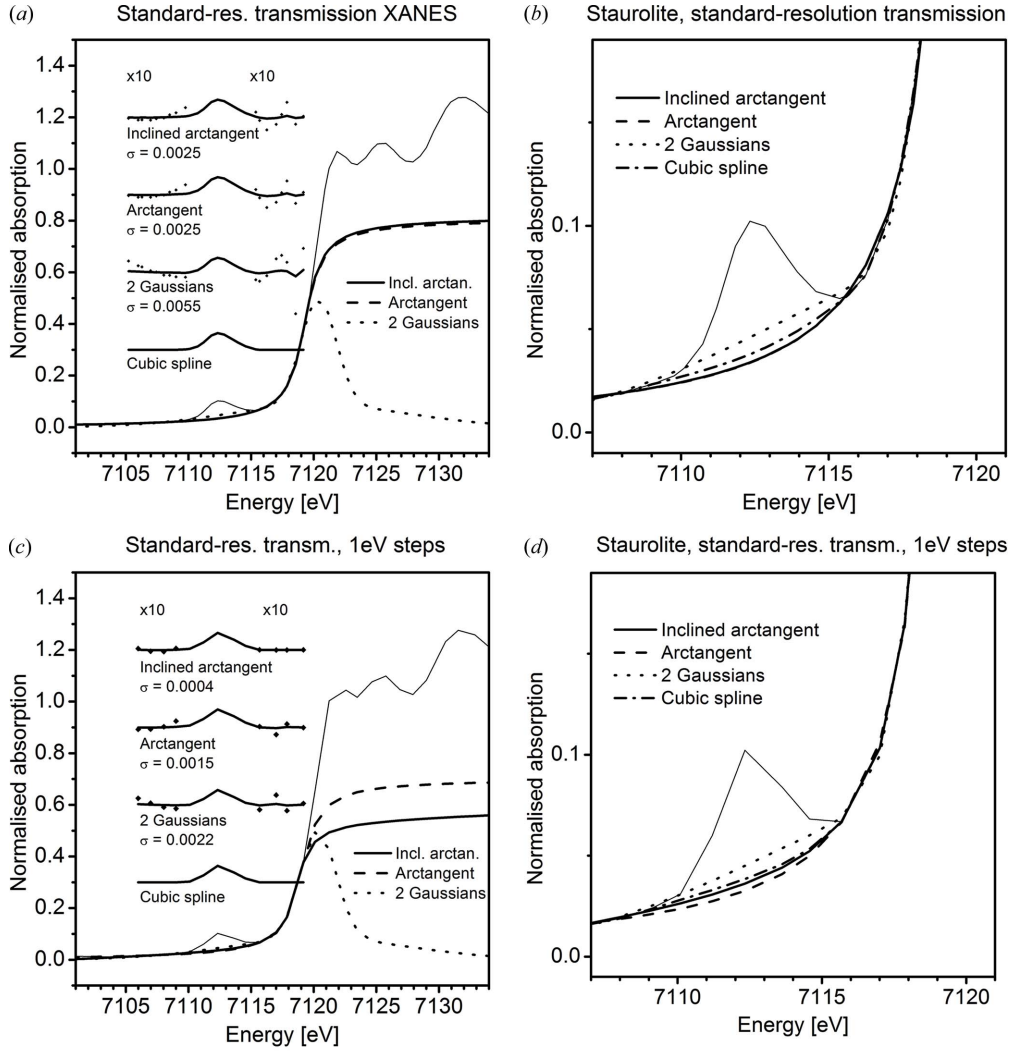

Figure 2
XANES spectra of staurolite and pre-edge extraction models for standard-resolution transmission-mode XANES data recorded in 0.5 eV increments (*a*) and the same data set with quality degraded by removing every second data point, resulting in 1 eV energy increments (*c*). The functions for modelling the edge onset, *i.e.* the inclined arctangent, arctangent, two Gaussian functions and cubic spline, are displayed with the XANES spectra they are applied to. The resulting extracted pre-edge peaks are shown offset for clarity. The fitting residuals are magnified by a factor of ten to show the misfit and the standard deviation (σ) is given. Details in the pre-edge region of plots (*a*) and (*c*) are shown in plots (*b*) and (*d*), respectively.

3.2. Effect of resolution on the pre-edge structure

In the next step, the potential of extracting the chemical structure of iron from standard-resolution data was evaluated by analysing pre-edge spectra recorded with both standard and high resolution. Graphical correlations between integrated intensities and the centroid positions of pre-edge features in a variogram were used to differentiate between different oxidation states and coordination geometries of iron [*cf.* pioneering work by Wilke *et al.* (2001) and other studies (Battiston *et al.*, 2003*b*; Heijboer *et al.*, 2004)]. The applicability of this method was first verified by applying it to pre-edge spectra of reference compounds containing known Fe species as well as to binary mixtures of these compounds. This approach was first tested using pre-edge spectra acquired with high resolution. Subsequently, to complement the above-mentioned studies, the variogram-based method was applied to pre-edge spectra measured with standard resolution, which is important for *operando* studies on catalysts, the main objective of this study.

Fig. 3 shows pre-edge spectra of the reference compounds staurolite, FeO, $FePO_4$ and α-Fe_2O_3 and their mechanical mixtures acquired with high resolution in transmission mode (the parent XANES spectra from which those pre-edge spectra were extracted are shown in Fig. S1 in the supporting information[1]). The pre-edge spectra of the reference compounds, extracted from XANES spectra measured in 0.5 eV energy increments, are shown in Fig. 4 along with pre-edge spectra of binary mixtures extracted from XANES spectra generated by merging absorption data of the reference compounds in various ratios. For each mixture series, one XANES spectrum was generated in precisely the same ratio as

[1] Supporting information for this paper is available from the IUCr electronic archives (Reference: RV5027).

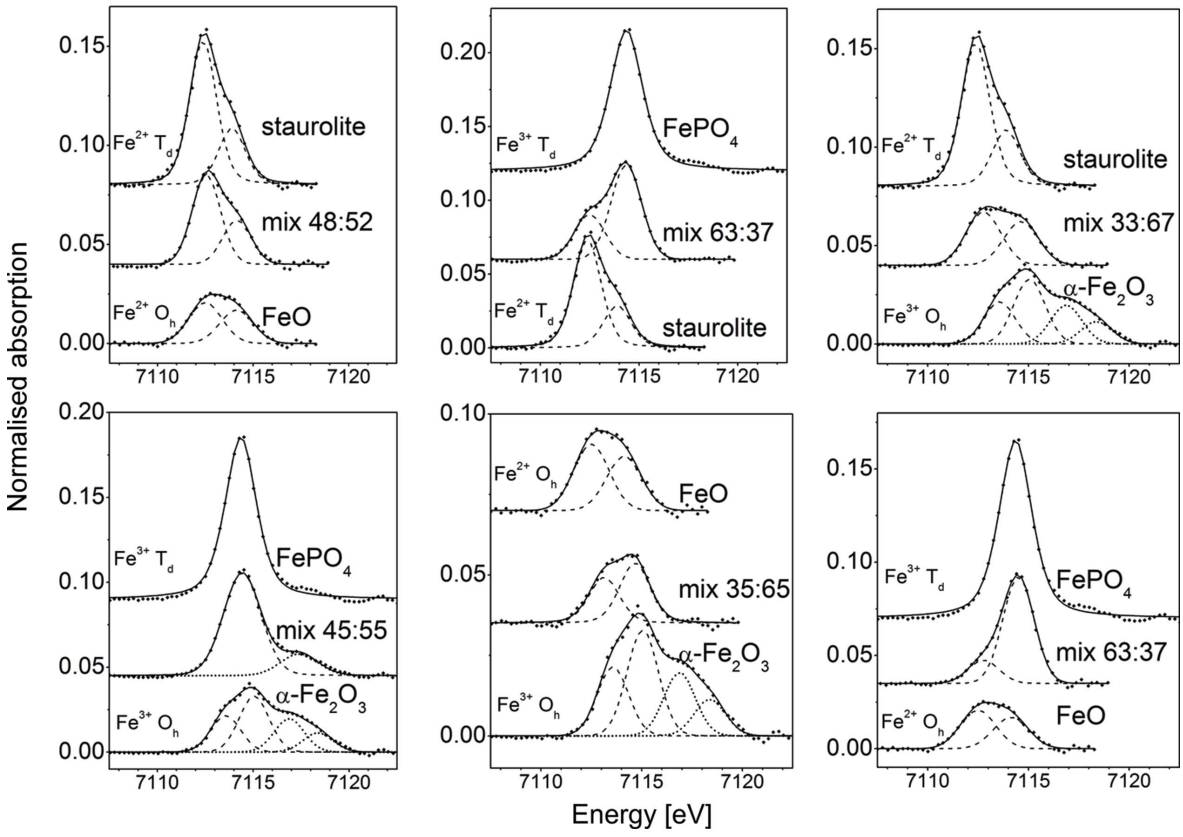

Figure 3
Pre-edge spectra of the reference compounds staurolite, FeO, $FePO_4$ and α-Fe_2O_3 and their binary mechanical mixtures from high-resolution transmission-mode XANES data, extracted using the inclined arctangent model function and fit with pseudo-Voigt peak functions. Transitions centred above 7115 eV (plotted in dotted lines) were omitted in the analysis. The parent XANES spectra are given in Fig. S1. The mixing ratios were determined using linear combination analysis of the normalized XANES spectra.

in the mixture measured with high resolution for direct comparison of the analysis as will be shown later. The parent XANES spectra (measured and merged) are shown in Fig. S2.

The pre-edge spectra were empirically deconvoluted using pseudo-Voigt peak functions and then compared with theoretically predicted electronic transitions (Table 2). The peak-fitting procedure must also be applicable when theoretical information of the electronic structure is not available. For this reason, peak fitting was applied to pre-edge spectra of the mixtures of reference compounds. This is especially useful for identification and isolation of non-local transitions, as will be shown in the following sections.

As the $1s \rightarrow 3d$ transition is a quadrupolar transition it is weak in intensity for coordination geometries with an inversion centre (centrosymmetric geometry), such as octahedral coordination. By changing the number and arrangement of ligands in fivefold or fourfold geometry, $3d$–$4p$ molecular orbital hybridization (mixing) is known to lead to facilitated dipolar transitions of the type $1s \rightarrow 4p$ with a significantly higher intensity (Westre *et al.*, 1997). A linear relationship between the degree of $3d$–$4p$ hybridization and the pre-edge intensity has been reported (Roe *et al.*, 1984) and thus a direct correlation of the pre-edge intensity and the local coordination number of the Fe ion could be obtained. Furthermore, the position of the pre-edge peak can be used as a direct measure of the Fe oxidation state, making an unambiguous distinction between Fe^{2+} (average pre-edge position 7112 eV) and Fe^{3+} (average pre-edge position 7113.5 eV) (Wilke *et al.*, 2001) possible. Note that the coordination geometry does not influence the pre-edge peak position in the case of Fe (Yamamoto, 2008).

The pre-edge spectra of the reference compounds staurolite (Fe^{2+} T_d), FeO (Fe^{2+} O_h) and $FePO_4$ (Fe^{3+} T_d) acquired with both high and standard resolution were fitted with two (staurolite, FeO) and one ($FePO_4$) pseudo-Voigt peaks, respectively (*cf.* Figs. 3 and 4), but with broader peak functions for the standard-resolution spectra (*cf.* Tables 2 and 3). The pre-edge spectrum of α-Fe_2O_3 was on the other hand deconvoluted into four peaks in the high-resolution spectrum and two peaks (2.9 eV FWHM, broader than the typical curve) in the standard-resolution spectrum. The use of four peaks (not shown) to fit the standard-resolution pre-edge spectrum of α-Fe_2O_3 had no positive effect on the quality of fit and led to identical numerical results. Deconvolution of the standard-resolution spectra required peaks with an average FWHM of 2.2 eV, in contrast to an average of 1.9 eV for the high-resolution spectra.

A distinctive feature of the pre-edge spectrum of α-Fe_2O_3 was the contribution above 7115 eV (plotted in dotted lines), which was attributed to transitions into the orbitals of the nearest-neighbour Fe atoms (non-local transitions), having mainly dipole character (Caliebe *et al.*, 1998; Glatzel *et al.*,

Table 2
Number, width (FWHM) and Gaussian fraction of the pseudo-Voigt peak functions used for fitting the pre-edge spectra of the reference compounds and their mechanical binary mixtures acquired in transmission mode with high resolution.

For the pure compounds, the electronic states resulting from crystal-field splitting of the free ion states are given. Final states marked in bold dominate in terms of intensity and are well identified in the pre-edge spectra.

Samples	Number of peaks	Free ion state → [final states]	FWHM (eV)	$x_{Gaussian}$ (%)
Staurolite (Fe^{2+} T_d)	2	$^4F \rightarrow [^4A_2\ \mathbf{^4T_2}\ ^4T_1]$, $^4P \rightarrow [\mathbf{^4T_1}]$	1.7	69
FeO (Fe^{2+} O_h)	2	$^4F \rightarrow [\mathbf{^4T_{1g}}\ ^4T_{2g}]$, $^4P \rightarrow [\mathbf{^4T_{1g}}]$	2.1	100
$FePO_4$ (Fe^{3+} T_d)	1	$^5D \rightarrow [^5E\ \mathbf{^5T_2}]$	1.9	44
α-Fe_2O_3 (Fe^{3+} O_h)	2 + 2†	$^5D \rightarrow [\mathbf{^5T_{2g}}\ \mathbf{^5E_g}]$	1.8	97

Mechanical mixtures	Ratio	Number of peaks	FWHM (eV)	$x_{Gaussian}$ (%)
Staurolite–FeO	48:52	2	1.8	100
$FePO_4$–staurolite	63:37	2	1.8	99
Staurolite–α-Fe_2O_3	33:67	2 + 0†	2.0	100
$FePO_4$–α-Fe_2O_3	45:55	1 + 1†	2.3	89
FeO–α-Fe_2O_3	35:65	2 + 0†	1.8	72
$FePO_4$–FeO	63:37	2	1.8	100

† The second number is the number of peaks centred above 7115 eV, being non-local transitions observed in the spectrum of α-Fe_2O_3 and mixtures containing α-Fe_2O_3, which are omitted in the analysis of the chemical state of Fe.

2009). These are irrelevant for probing the first Fe–O coordination shell. An important reason for fitting the pre-edge spectra was to eliminate these contributions prior to further analysis (Wilke *et al.*, 2001; Battiston *et al.*, 2003*a*). The two-peak fit provided the same proportion of local and non-local contributions (1 and 1) as the four-peak fit (2 and 2) (*cf.* Figs. 3 and 4).

Crystal-field theory predicts final electronic states of the Fe ion in different oxidation states and coordination geometries, which are probed by transitions corresponding to pre-edge features. For the Fe species in the reference compounds the final states of these transitions are given in Table 2, but typically fewer peaks were sufficient to deconvolute the spectra. For example, a total of four final states ($[^4A_2\ ^4T_2\ ^4T_1]$ and $[^4T_1]$) were found in the spectrum of staurolite, but only two were clearly identified, probably, the $^4T_2$ and $^4T_1$ states marked bold, as transitions to these states are the most intense (Westre *et al.*, 1997). Statistically, the fits could not be improved significantly by using more peaks. Besides, the number of peaks should not play a role in the variogram-based pre-edge analysis (shown later), since this does not have an influence on the complete integrated area and average position of the pre-edge peak. Also, the Gaussian fraction in the pseudo-Voigt profiles was allowed to float during the decon-

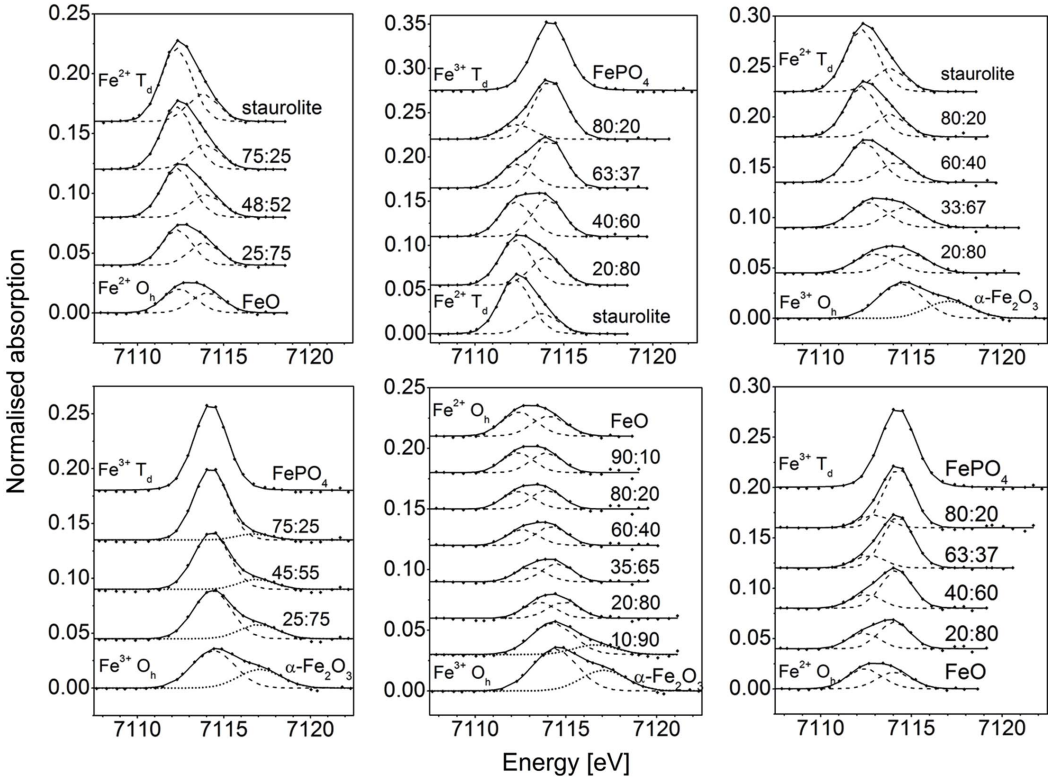

Figure 4
Pre-edge spectra of the reference compounds staurolite, FeO, $FePO_4$ and α-Fe_2O_3 and their binary mixtures from standard-resolution transmission-mode XANES data, extracted using the inclined arctangent model function and fit with pseudo-Voigt peak functions. Transitions centred above 7115 eV (plotted in dotted lines) were omitted in the analysis. The parent XANES spectra can be viewed in Fig. S2; the mixture spectra were generated by merging normalized XANES spectra of the pure reference compounds in the specified ratios.

Table 3
Number, width (FWHM) and Gaussian fraction of the pseudo-Voigt peak functions used for fitting the pre-edge spectra of the reference compounds acquired in transmission mode with standard resolution.

	Samples	Number of peaks	FWHM (eV)	$x_{Gaussian}$ (%)
Fe^{2+} T_d	Staurolite	2	2.1	95
	Ceylonite $(Mg,Fe)Al_2O_4$	2	2.5	87
Fe^{2+} O_h	FeO	2	2.2	89
	Fe(II)oxalate	2	2.2	51
	$FeCO_3$	2	2.4	75
	Olivine $(Mg,Fe)_2SiO_4$	2	2.4	67
	Bronzite $(Mg,Fe)_2Si_2O_6$	2	2.3	50
Fe^{3+} T_d	$FePO_4$	1	2.3	83
	Sanidine	2	2.3	99
Fe^{3+} O_h	α-Fe_2O_3	1 + 1†	2.9	100
	$FePO_4{\cdot}xH_2O$	2	2.3	93
	Fe(III)acac	2	2.1	97
	$Fe(NO_3)_3{\cdot}9H_2O$	2 + 1†	2.1	67
	Aegirine $NaFeSi_2O_6$	2	2.2	78
Others	γ-Fe_2O_3 (Fe^{+3}, T_d and O_h)	1 + 1†	2.6	99
	Fe_3O_4 (Fe^{+2}, Fe^{+3}, T_d and O_h)	2 + 1†	2.3	100
	Fe(II) phthalocyanine	1 + 1†	2.6	87

† The second number is the number of peaks centred above 7115 eV, being non-local transitions observed in the spectrum of α-Fe_2O_3 and mixtures containing α-Fe_2O_3, which are omitted in the analysis of the chemical state of Fe.

volution to achieve a statistically reasonable fit. This resulted in rather high values due to the instrumental broadening. Owing to the uncertainties introduced with this empirical approach, the Gaussian fraction was not correlated to the peak width (FWHM), as otherwise predicted (Farges *et al.*, 2004).

The pre-edge spectra of binary mixtures of the reference compounds acquired with high and standard resolution were all adequately deconvoluted using two peak functions (Figs. 3 and 4), with larger broadening (FWHM) for standard resolution (*cf.* Tables 2 and 3). Pre-edge spectra of mixtures containing α-Fe_2O_3 were fitted with either two broad peaks, one assigned to local transitions and the second to non-local transitions when identified, as, for example, in $FePO_4$–α-Fe_2O_3 mixtures, or two narrow peaks both assigned to local transitions, as, for example, in FeO–α-Fe_2O_3 mixtures.

In the pre-edge variogram in Fig. 5(*a*), the sets of points corresponding to Fe^{2+} and Fe^{3+} oxidation states and T_d and O_h geometries were clearly distinguished in line with Wilke *et al.* (2001). The separation of the centroid positions by *ca* 1.5 eV and the distinct integrated intensities of the pre-edge spectra, approximately 0.1 for O_h geometry and above 0.2 for T_d geometry, form a sound basis for accurate analysis of oxidation state and coordination geometry of iron. The centroid position in the pre-edge spectrum of FeO was at higher energies compared with that of staurolite, indicating that FeO contains traces of Fe^{3+} (Hazen & Jeanloz, 1984). In the variogram for standard-resolution pre-edge spectra (Fig. 6*a*), the data points corresponding to the reference compounds were very well reproduced compared with those obtained from high-resolution spectra.

The points in the variogram corresponding to the six sets of binary mixtures of the reference compounds were located in between the points corresponding to the pure reference

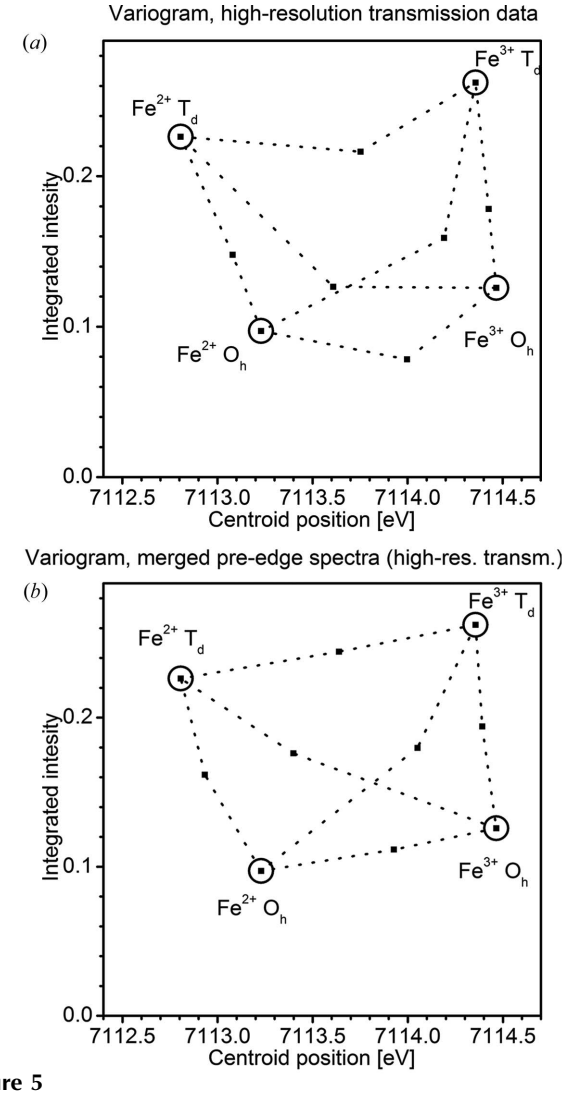

Figure 5
Pre-edge variogram of the integrated intensity and centroid position for the reference compounds staurolite, FeO, $FePO_4$ and α-Fe_2O_3 and their binary mechanical mixtures shown in Fig. 3. The points for the binary mixtures in the variogram in (*a*) originate from the extracted pre-edge spectra of the mixed compounds. The corresponding points in the variogram in (*b*) are based on the 50:50 linear combinations of the already extracted pre-edge spectra of the pure reference compounds. The peak width (FWHM) and Gaussian fraction ($x_{Gaussian}$) of the pseudo-Voigt functions used for peak fitting are presented in Table 2.

compounds, but with significantly lower intensity. This was observed for both high- and standard-resolution data [Figs. 5(*a*) and 6(*a*), respectively]. This decrease in intensity could be due to the close overlap of the steep edge onset with the pre-edge peak, which is seen in, for example, the XANES spectra of FeO–α-Fe_2O_3 mixtures in Fig. S2(*b*). The portion of the pre-edge peak that overlaps with the edge and is being subtracted can be a significant fraction of the pre-edge peak intensity, but is negligible in comparison with the value of the main edge. The strong decrease in intensity can be directly observed in the pre-edge spectra of, for example, the 35:65 and 20:80 mixtures of FeO and α-Fe_2O_3 (Fig. 4). This effect is minimised when the pre-edge peak is well separated from the edge onset, such as in HERFD-XANES spectra.

In literature, it was reported that the extracted pre-edge spectra of mixed compounds cannot be properly described by linear combinations of pre-edge spectra of the pure compounds (Berry *et al.*, 2003), as is possible with full XANES spectra. To demonstrate the effect of edge subtraction from the XANES spectra on the pre-edge variogram, another variogram was constructed, where the pre-edge spectra of the mixtures were merely calculated as linear combinations of the pre-edge spectra of the pure compounds, instead of subtracting the edge onset from XANES spectra of each mixture individually. The variograms based on linear combinations (ratio 50:50) of high-resolution pre-edge spectra (Fig. 5*b*) and those of standard-resolution pre-edge spectra (ratios 20:80, 40:60, 60:40 and 80:20; Fig. 6*b*) showed almost no decrease in intensity, verifying that an apparent decrease of the pre-edge intensity is caused by subtraction of the overlapping edge onset.

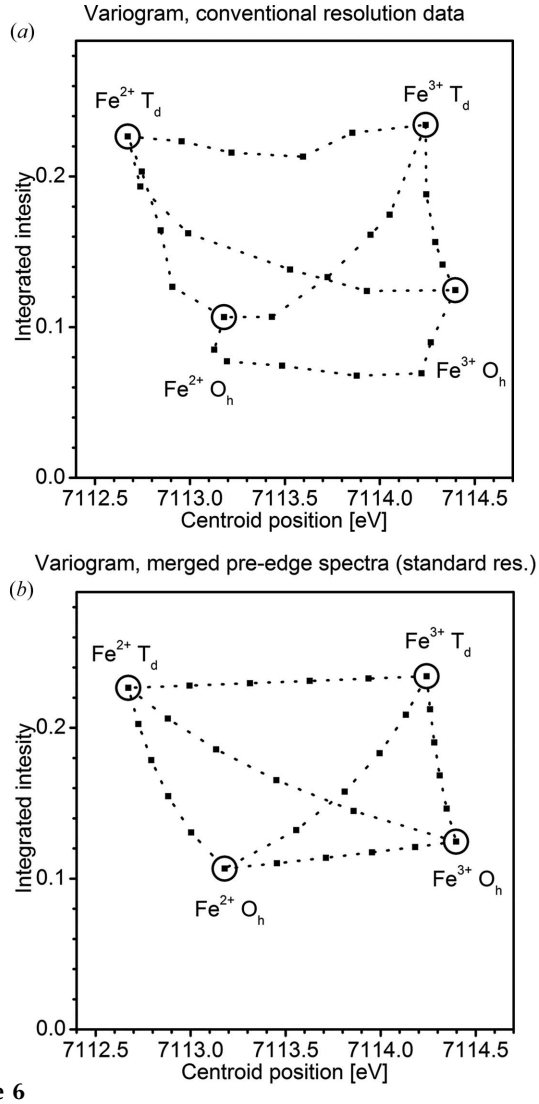

Figure 6
Pre-edge variogram of the integrated intensity and centroid position for the reference compounds staurolite, FeO, $FePO_4$ and α-Fe_2O_3 and their binary mixtures shown in Fig. 4. The points for the binary mixtures in the variogram in (*a*) originate from the extracted experimental pre-edge spectra of the mixed compounds. The corresponding points in the variogram in (*b*) are based on the linear combinations (ratios 20:80, 40:60, 60:40 and 80:20) of the already extracted pre-edge spectra of the pure reference compounds. The peak width (FWHM) and Gaussian fraction ($x_{Gaussian}$) of the pseudo-Voigt functions used for peak fitting are presented in Tables 3 and 4.

Table 4
Number, width (FWHM) and Gaussian fraction of the pseudo-Voigt peak functions used for fitting the standard-resolution pre-edge spectra of the binary mixtures of selected reference spectra.

Mixed XANES spectra	Ratio	Number of peaks	FWHM (eV)	$x_{Gaussian}$ (%)
Staurolite–FeO	75:25	2	2.2	92
	48:52	2	2.2	97
	25:75	2	2.1	100
$FePO_4$–staurolite	80:20	2	2.2	97
	63:37	2	2.1	100
	40:60	2	2.1	98
	20:80	2	2.1	97
Staurolite–α-Fe_2O_3	80:20	2 + 0†	2.1	91
	60:40	2 + 0†	2.2	100
	33:67	2 + 0†	2.4	89
	20:80	2 + 0†	2.6	100
$FePO_4$–α-Fe_2O_3	75:25	1 + 1†	2.3	99
	45:55	1 + 1†	2.4	97
	25:75	1 + 1†	2.6	100
FeO–α-Fe_2O_3	90:10	2 + 0†	2.1	99
	80:20	2 + 0†	2.0	99
	60:40	2 + 0†	2.0	97
	35:65	2 + 0†	1.9	98
	20:80	2 + 0†	2.0	100
	10:90	1 + 1†	2.7	96
$FePO_4$–FeO	80:20	2	1.9	96
	63:37	2	2.0	93
	40:60	2	2.0	90
	20:80	2	2.0	100

† The second number is the number of peaks centred above 7115 eV, being non-local transitions observed in the spectrum of α-Fe_2O_3 and mixtures containing α-Fe_2O_3, omitted in the analysis of the chemical state of Fe.

The variogram-based analysis of standard-resolution pre-edge spectra does not differ from that of high-resolution spectra, as the same trends are seen in both. This makes it an attractive approach for *operando* studies on catalysts as well. Additionally, the total integrated area of the pre-edge peak is not affected by the difference in resolution, meaning that the results obtained with high and standard resolution can be analysed in a single variogram. The standard deviation in the integrated area was ± 0.013, determined statistically by comparing the integrated intensities of the pre-edge spectra of the reference compounds and of the binary mixtures with the same stoichiometric ratios, acquired with both high and standard resolution. The effect of the spectral resolution on the centroid position in the variogram was also investigated: compared with high-resolution spectra, the centroid position of standard-resolution pre-edge spectra is systematically shifted to lower energy by 0.12 ± 0.06 eV, although all spectra were calibrated using the first inflection point in the XANES spectrum of a Fe foil. This shift most probably occurs because the high-energy tail of the pre-edge peak is very weak compared with the edge onset and is therefore truncated along with the edge during the extraction. The area-based average position of the extracted peak thus shifts to lower energies. This small shift can be noticed by a comparison of the vario-

grams [Figs. 5(*a*) and Fig. 6(*a*)], but remains practically undetected when comparing the entire pre-edge spectra (Figs. 3 and 4).

3.3. Accuracy of pre-edge analysis validated by further reference compounds

In a next step the results from the previous sections were applied to reference compounds that partly contain several Fe species, which is also typical for heterogeneous catalysts. Before applying the pre-edge analysis method to such unknown systems, it is important to know how accurately the oxidation state and the coordination geometry can be quantified. Hence, a collection of different Fe-containing reference compounds with specific chemical states of Fe was investigated (Table 1). The varying chemical composition has a large impact on the shape of the parent XANES spectra [Fig. S3(*a*)] above the absorption edge, which probes multiple-scattering of low-energy photoelectrons. Nevertheless, the pre-edge spectra [Fig. 7; detail in the XANES spectra Fig. S3(*b*)] specifically reflect the chemical speciation of iron in these compounds, as shown in the variogram in Fig. 8. However, variations within the same chemical state of Fe are present. For example, the pre-edge peak in the ceylonite spectrum is slightly wider and shifted to higher energies as compared with that of staurolite (both Fe^{2+} in T_d symmetry).

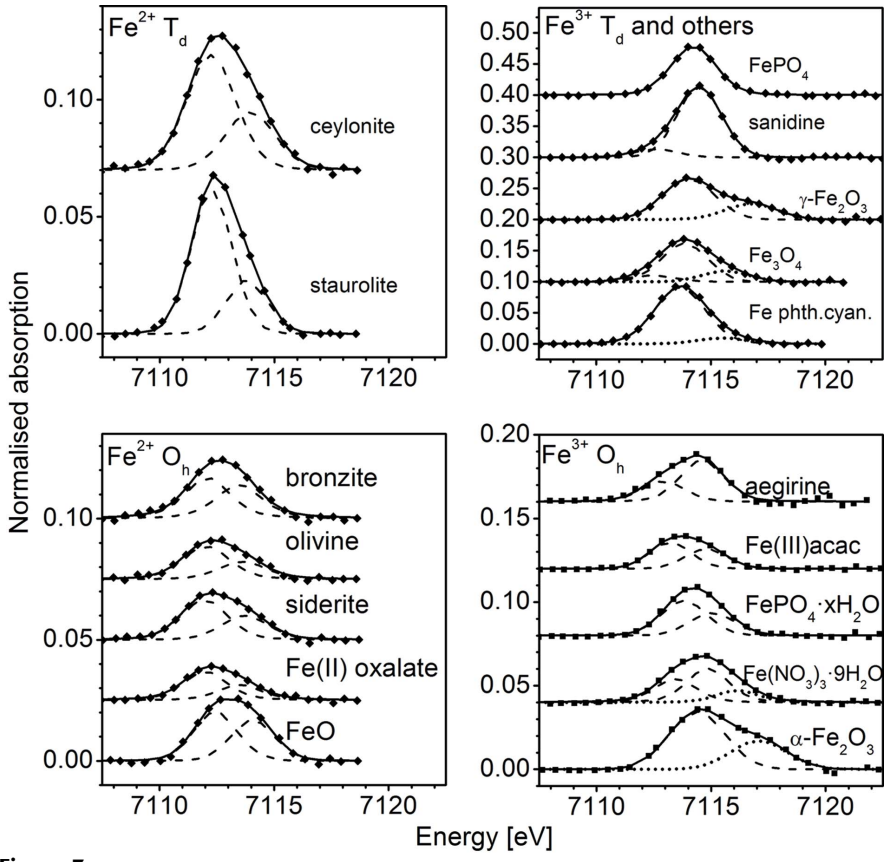

Figure 7
Pre-edge spectra of reference compounds extracted from standard-resolution transmission-mode XANES data, summarized in Table 3. Extraction was carried out using the inclined arctangent model function and the pre-edge spectra were fit with pseudo-Voigt peak functions. Transitions centred above 7115 eV (plotted in dotted lines) were omitted in the analysis. The parent XANES spectra can be viewed in Fig. S3.

Variations in the pre-edge spectra were also observed for compounds with Fe^{2+} in O_h geometry, most remarkable for FeO (circled) due to possible Fe^{3+} impurities. The integrated area also varies, which is in part influenced by the subtraction of the edge onset.

A large intensity variation in the pre-edge spectra of $FePO_4$ and sanidine (Fe^{3+} in T_d symmetry) suggests a partial deviation from T_d geometry of iron in $FePO_4$. The high integrated intensity of the sanidine spectrum is consistent with previously reported values for tetrahedral Fe^{3+} (Wilke *et al.*, 2001), while the intensity found for $FePO_4$ was lower than expected. The coordination geometry of dehydrated $FePO_4$ is tetrahedral, but becomes octahedral when H_2O molecules are included in the lattice, which cannot be excluded here.

Interesting variations were observed in the pre-edge spectra of Fe^{3+} O_h compounds. The spectra of aegirine, Fe(III)acac and $FePO_4.xH_2O$ were fitted with two peak functions of varying intensity ratios. A third high-energy peak was found in the pre-edge spectrum of $Fe(NO_3)_3.9H_2O$, which was omitted in the analysis as a non-specific transition as it was centred

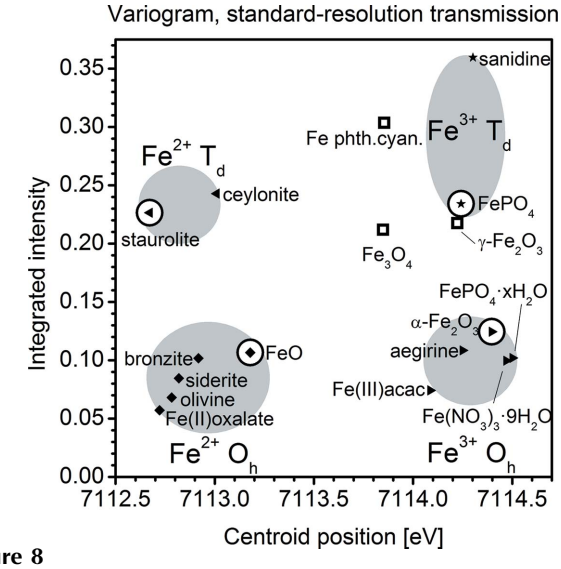

Figure 8
Pre-edge variogram for spectra of reference compounds, which are shown in Fig. 7. Circled data points correspond to the four references samples covered in detail in the previous sections. Grey areas highlight the groups of points corresponding to the four types of Fe species. The uncertainties determined graphically from this plot are ± 0.2 eV in centroid position and ± 0.03 in integrated intensity. The peak width (FWHM) and Gaussian fraction ($x_{\rm Gaussian}$) of the pseudo-Voigt functions used for peak fitting are presented in Table 3.

above 7115 eV. The spectrum of α-Fe_2O_3 was fitted with two peaks as discussed in the previous sections, one for local and one for non-local transitions.

The data points in the variogram in Fig. 8 originating from the reference compounds representing the four end-member states of Fe ions (Fe^{2+} and Fe^{3+} in T_d and O_h geometries) are distributed in four groups, each related to its specific type of Fe species. Thus, the variogram can be used to distinguish between Fe^{2+} and Fe^{3+} as well as between the geometries, independent of the total chemical composition, which is in line with Wilke *et al.* (2001). Based on the pre-edge spectra of the compounds with Fe^{2+} and Fe^{3+} in O_h symmetry, an uncertainty of ± 0.2 eV in the centroid position and ± 0.03 for the intensity was estimated. The encircled points represent the four reference compounds staurolite, FeO, $FePO_4$ and α-Fe_2O_3 which were presented in the previous sections to illustrate the trends in pre-edge analysis. These data points suffer from the already mentioned uncertainties (*e.g.* FeO due to presumed contamination by Fe^{3+}), but are representative of the different chemical states of iron.

Using the established correlations, three compounds of other chemical speciation of iron (Table 1) were analysed. Maghemite (γ-Fe_2O_3) formally has a defect spinel structure and Fe^{3+} distributed among T_d and O_h sites. This compound exhibited a XANES spectrum similar to that of α-Fe_2O_3 as both are pure oxides of Fe^{3+} (Fig. S3), but with higher pre-edge peak intensity due to the presence of tetrahedrally coordinated Fe ions. The pre-edge peak (Fig. 7) was fitted with a main contribution centred at 7114.2 eV and a shoulder above 7115 eV. The main peak contains overlapping features corresponding to the transitions observable for Fe^{3+} species in T_d and O_h sites. The high-energy shoulder was attributed to non-local transitions observed in pre-edge spectra of trivalent metal ions due to metal–metal interactions (de Groot *et al.*, 2009) and was omitted in the analysis. In the variogram (Fig. 8), the data points of maghemite were placed at 7114.2 eV as expected for compounds containing pure Fe^{3+}, with intensity slightly below that of the $FePO_4$ reference, clearly pointing at a mixture of T_d and O_h sites.

The structure of magnetite (Fe_3O_4) is an inverse spinel similar to that of maghemite, formally with the Fe atoms equally distributed as Fe^{2+} at O_h sites, Fe^{3+} at O_h sites and Fe^{3+} at T_d sites. In fact, the mixture of oxidation states is consistent with the position of the edge at lower energies than that typical for Fe^{3+}, but higher than that for Fe^{2+} (Fig. S3). Regarding the pre-edge spectrum, three peaks satisfactorily fitted this spectrum (Fig. 7). The first weak peak at *ca* 7112 eV was a contribution from Fe^{2+} at O_h sites [presumably due to the $^4T_{1g}(^4F)$ state], the second peak mainly contained contributions from the intense $^5T_2(^5D)$ state of Fe^{3+} at T_d sites and a third peak above 7115 eV, assigned to non-local transitions, and omitted. The position of magnetite in the variogram (Fig. 8) was consistent with the electronic speciation of the Fe ions, but further quantification would be limited by uncertainties of the analysis.

The coordination compound iron phthalocyanine formally contains a divalent Fe ion coordinated in square planar geometry by four N atoms of the tetradentate phthalocyanine ligand. The position of the absorption edge (Fig. S3) and the pre-edge spectrum (Fig. 7) strongly suggested a large fraction of Fe^{3+} in the compound, reflecting that the formally assumed valence of the Fe ion was inaccurate. Oxidation from Fe^{2+} to Fe^{3+} could have occurred during the preparation of the sample. The high intensity of the pre-edge peak is due to the strong $3d$–$4p$ hybridization, which for square planar geometry is known to be as high as that for tetrahedral geometry (Westre *et al.*, 1997; Wilke *et al.*, 2001).

The three test compounds demonstrate that the procedure presented in this work provides the chemical state and the distribution of site geometries from pre-edge spectra, even if acquired with standard resolution. The precision of this method is, however, limited and pre-edge analysis is well suited as a complementary technique for confirming the nature of Fe species.

3.4. Evolution of Fe species in 1% Fe/Al_2O_3 and 0.5% Fe/BEA catalysts during reduction

Finally, pre-edge analysis was applied to a typical *in situ* study of a 1% Fe/Al_2O_3 and 0.5% Fe/BEA zeolite catalyst during temperature-programmed reduction in 5% H_2/He (Figs. 9, 10 and 11). These demonstrate two cases: one with a high degree of noise in the XANES spectra due to rapid data acquisition, the low Fe content and fluctuations in the edge jump. The latter effect can be seen above the edge, as the spectra tend to group instead of being evenly spaced in the stacked plot in Fig. 9(*a*). The second case (Fig. 11) is data with better quality.

At first, linear combination analysis (LCA) of the XANES spectra was performed. For this purpose, XANES spectra of the initial and the final state of the Fe/Al_2O_3 catalyst were used, each one merged of several data sets in order to increase the signal-to-noise ratio (Fig. 9*a*, bottom). The LCA results (Fig. 10*c*) indicate a transformation between two states, assumed to be Fe^{3+} and Fe^{2+}. All spectra could be well fit as linear combinations of the initial and final spectrum. Isosbestic points indicated that the structural transformation of the Fe sites occurred in one step.

The corresponding pre-edge spectra are shown in Fig. 9(*b*). Although the pre-edge region was affected by a certain level of noise, it could be successfully extracted and fitted with a single pseudo-Voigt function. The pre-edge spectra measured between 26 and 310°C are almost identical and are modelled by a pseudo-Voigt peak of 2.5 eV width positioned at 7114.4 eV which is characteristic of Fe^{3+}. The high intensity of this peak indicates non-centrosymmetric geometry, as the pre-edge variogram in Fig. 10(*a*) shows. The integrated intensity is between that of pre-edge spectra of $FePO_4$ and sanidine, which were used as Fe^{3+} references for the T_d geometry, and the peak is similar or slightly wider (2.3 eV, Table 3). The Fe^{3+} ions in the Fe/Al_2O_3 catalyst can thus be assumed to be mainly in a tetrahedral or similar geometry, but most probably in a mixture of four- and five-fold coordination. In this case, a single peak accounts for all transitions which are present, but

not individually resolved within the pre-edge feature. The surface species of Fe in the catalyst can be rather disordered (Boubnov *et al.*, 2013) and the Fe ion site can probably not be described by a single well defined structure model.

Upon the structural transformation between 300 and 500°C, the pre-edge peak shifts to lower energies [Figs. 10(*b*) and 10(*c*), marked by grey lines]. Around 400°C, halfway in the $Fe^{3+} \rightarrow Fe^{2+}$ transformation, the pre-edge peak centred at 7113.7 eV increases in width to 3.2 eV, and the Gaussian fraction of the pseudo-Voigt peak function increases to 100%. The Gaussian/Lorentzian character of the peak functions is, however, subject to large errors, as described previously. Once the chemical transformation is complete, the peak width again decreases to 2.5 eV and is located at *ca* 7112.8 eV, characteristic of Fe^{2+} species. The broadening of the pre-edge peak during the transformation is attributed to overlapping pre-edge spectra of the initial and final state. The final state of the Fe sites could be described as four- to five-fold coordinated Fe^{2+} (between the four-fold and six-fold coordinated Fe^{2+} reference points in the variogram). In fact, during the entire transformation, the coordination is conserved as four- to five-fold.

For comparison, an analogous TPR study of a 0.5% Fe/BEA catalyst is presented in Fig. 11. In contrast to the study of the Fe/Al_2O_3 catalyst, the XANES spectra (Fig. 11*a*) were acquired with higher resolution and better quality (0.1 eV energy increments). The pre-edge spectra extracted using the inclined arctangent function could be fitted with one or two pseudo-Voigt peaks: a double feature fitted with two peaks of 2.9 eV FWHM was easily distinguished after Fe was reduced to Fe^{2+} [Figs. 11(*b*) and 11(*d*)], but the pre-edge of the initial oxidized Fe^{3+} species was best fitted with a single peak of 2.0–2.5 eV FWHM. Attempts to apply a two-peak fit resulted in the overlap of the two peaks. At all times, the pseudo-Voigt functions took on a highly (>90%) Gaussian character (Fig. 11*d*).

The variogram in Fig. 11(*c*) is very similar to the one for Fe/Al_2O_3, showing a reduction of Fe^{3+} to Fe^{2+}, maintaining a local coordination number of *ca* 5. The transition is halfway through at about 315°C, and when the experiment is finished at 393°C the reduction is only about 80% complete, because the pre-edge centroid does not reach 7112.6 eV, characteristic of pure Fe^{2+}. The good reducibility at low temperature of the Fe/BEA catalyst with respect to the Fe/Al_2O_3 has shown to be correlated to a high catalytic activity for NO_x removal by selective catalytic reduction with ammonia (NH_3-SCR) (Boubnov *et al.*, 2013).

The simultaneous analysis of the oxidation state and local coordination number embraces also valuable information in HERFD-XANES data. In fact, the pre-edge analysis procedure in the present work was recently applied to study a Fe/ZSM-5 catalyst during NH_3-SCR and under relevant reaction conditions, acquiring combined HERFD-XANES and valence-to-core X-ray emission spectra (Boubnov *et al.*, 2014). Under the series of oxidizing and reducing atmospheres applied to the catalyst sample, the Fe sites took on average oxidation states between Fe^{2+} and Fe^{3+}, maintaining a local coordination number of *ca* 4–5. The intensity of the pre-edge peak in HERFD-XANES spectra, detecting the fluorescence with high resolution at the Fe $K\beta_{1,3}$ line, was approximately twice as high as that reported herein for transmission and standard-resolution fluorescence XANES data. For establishing a vario-

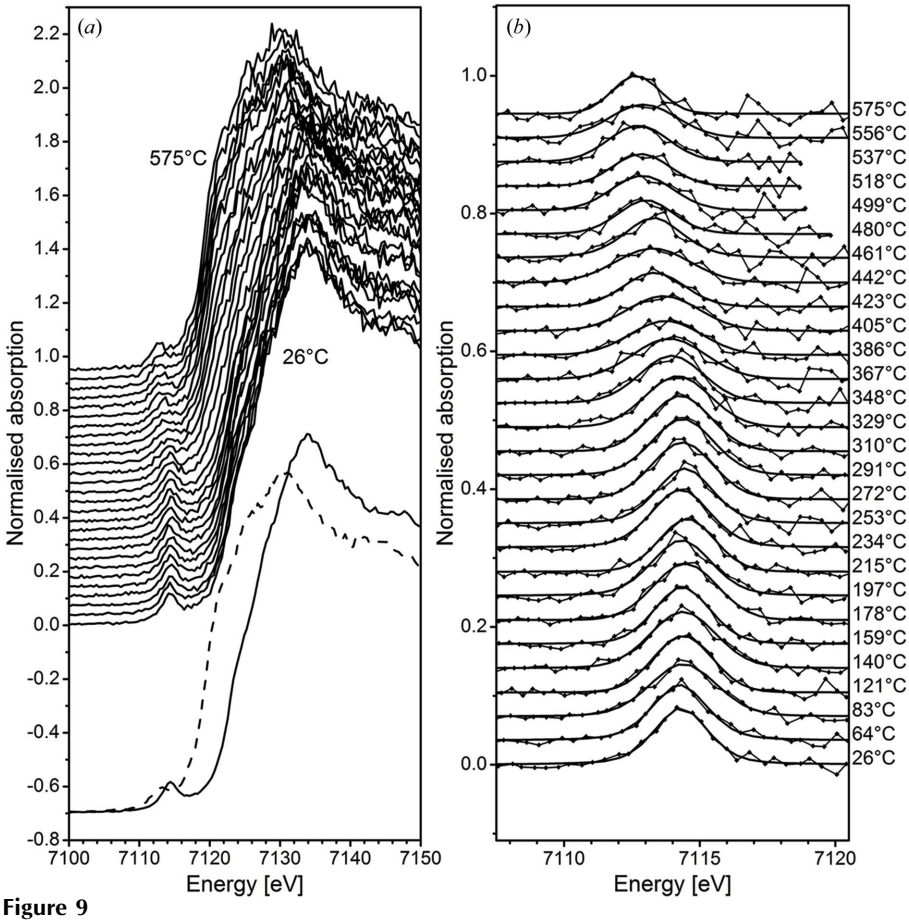

Figure 9
In situ Fe *K*-edge XANES spectra (*a*) and the pre-edge spectra (*b*) of a 1% Fe/Al_2O_3 catalyst acquired during a TPR experiment with standard resolution in fluorescence mode. The spectra were acquired using continuous energy scans with a period of approximately 4 min per spectrum. The catalyst powder was exposed to a flow of 5% H_2/He (50 ml min^{-1}) in a quartz capillary microreactor and heated from room temperature to 575°C at a linear rate of 5°C min^{-1}. The spectra of the starting state (solid line) and final state (dashed line) are shown together in (*a*); these were used as the basis for linear combination analysis of the whole series of the XANES spectra. The pre-edge spectra in (*b*) were extracted using the inclined arctangent function and fit with a single pseudo-Voigt peak function. The peak width (FWHM) and Gaussian fraction ($x_{Gaussian}$) of the pseudo-Voigt functions are presented graphically in Fig. 10(*b*).

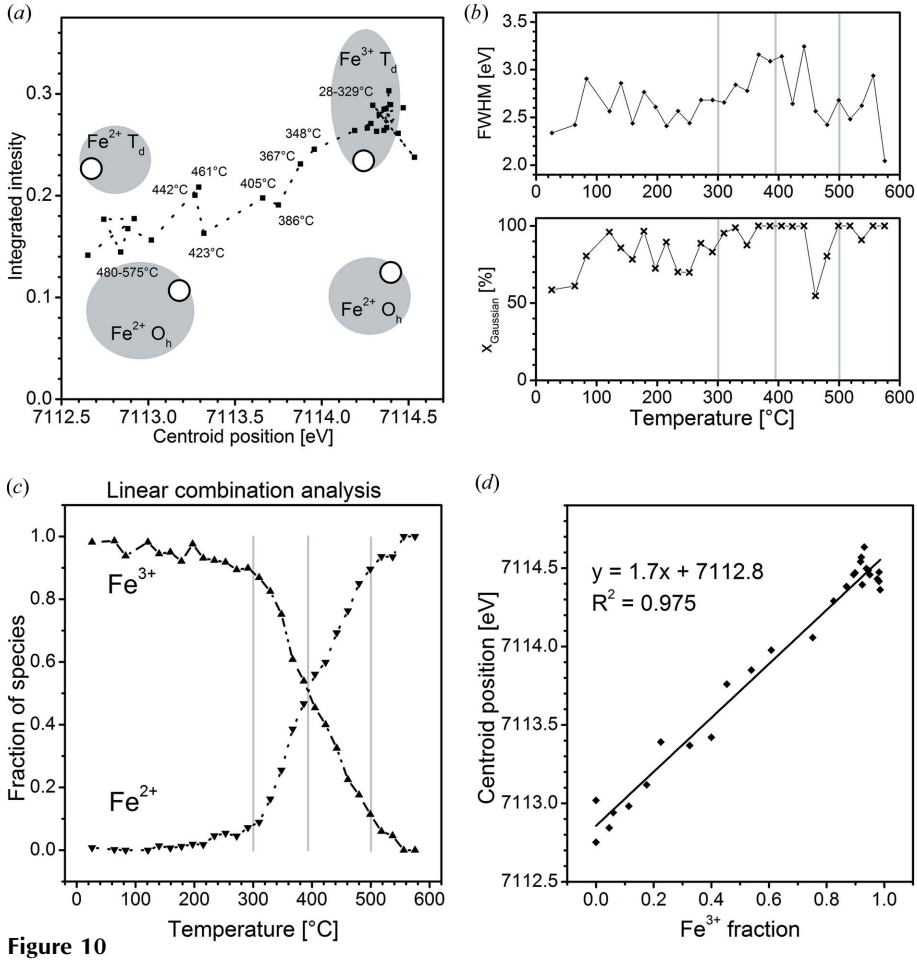

Figure 10
Analysis of the *in situ* pre-edge spectra of the 1% Fe/Al_2O_3 catalyst depicted in Fig. 9(*b*). (*a*) Variogram of the total integrated intensity and centroid position of the pre-edge peak at different temperatures of the TPR experiment, compared with data points of the reference compounds staurolite, FeO, $FePO_4$ and α-Fe_2O_3 from spectra measured with standard resolution (marked with circles and the grey fields for the four types of Fe species given in Fig. 8). (*b*) Evolution of the peak width (FWHM) and Gaussian fraction ($x_{Gaussian}$) of pseudo-Voigt functions as a function of temperature. (*c*) Fraction of Fe^{3+} and Fe^{2+} species as a function of temperature as estimated from linear combination analysis [the first XANES spectrum is assumed to be Fe^{3+} and the last XANES spectrum is assumed to be Fe^{2+}, carried out between 7105 eV and the isosbestic point at 7132 eV seen in Fig. 9(*a*)]. (*d*) Linear relationship between the fraction of Fe^{3+} species calculated by LCA and the pre-edge centroid position. The grey lines in (*b*) and (*c*) indicate the temperatures where the transformation of Fe^{3+} to Fe^{2+} has advanced *ca* 10%, 50% and 90% to guide the eye.

gram, the XAS spectra of reference samples must be acquired in the HERFD mode, but the study demonstrates in general the advantageous approach also in catalysis.

Variogram-based pre-edge analysis will be in general a valuable approach in XAS studies, *e.g.* those reported by Høj *et al.* (2009), Klukowski *et al.* (2009), Maier *et al.* (2011), Bordiga *et al.* (2013), Liu *et al.* (2013, 2014), Tepluchin *et al.* (2014) and Doronkin *et al.* (2014*b*), providing further information about oxidation state and geometry also under *operando* conditions.

The LCA results can be correlated with the pre-edge analysis results for quantifying the Fe oxidation state in similar chemical systems. Calibrations of the pre-edge centroid position and the fraction of Fe^{3+} species, especially with application to geology and studies of historical items, are reported for various Fe-containing materials using standard-resolution data (Berry *et al.*, 2003; Schmid *et al.*, 2003) and high-resolution data (Wilke *et al.*, 2005, 2009; Cottrell *et al.*, 2009). Fig. 10(*d*) shows a linear relationship between the Fe oxidation state in terms of the Fe^{3+} fraction and the pre-edge centroid position. From this relationship, the fraction of Fe^{3+} species in a mixture of Fe^{2+} and Fe^{3+} can be determined merely from the pre-edge centroid position within an error of *ca* 10%. The determination of the oxidation state of Fe can thus be carried out by both pre-edge analysis and LCA. The latter is a simple and common method in catalysis (Pirngruber *et al.*, 2004; Høj *et al.*, 2009), where the spectra of the fully oxidized and fully reduced catalyst are used as standards. However, a disadvantage of LCA is that XANES spectra of well defined reference compounds such as bulk oxides cannot adequately reproduce the XANES features of the catalysts, which have unique spectral features for each chemical system. Hence, a full reduction of each catalyst system must be carried out to reach the final state and use the corresponding spectrum as specific reference. Moreover, the pre-edge spectrum simultaneously probes the geometry of the Fe species, which is important for the identification of the role of the Fe centres for the catalytic reaction (Battiston *et al.*, 2003*b*). On the other hand, reliable reference samples are needed for this analysis and the results are subject to a certain error.

Another established method is the use of the edge position (Berry *et al.*, 2003; Maier *et al.*, 2011), as this is directly affected by the oxidation state. This method has its advantages when pre-edge analysis becomes difficult due to the low intensity of the pre-edge peak occurring for octahedrally coordinated Fe and a high noise level (Maier *et al.*, 2011). In fact, the pre-edge method suffers when analysing low-intensity pre-edge spectra due to distortions in the pre-edge variogram (Fig. 6*a*). For analysis of the edge position, the oxidation state must be calibrated with respect to the edge position. However, since the characteristics of the XANES spectra may vary for different chemical systems, each type of chemical system must be considered individually. In contrast, pre-edge analysis is potentially independent of the chemical system within the oxidation states and coordination geometries discussed in the present work. Further difficulties associated with the use of the edge position are due to the fact that the edge of a Fe *K*-edge XANES spectrum can have several

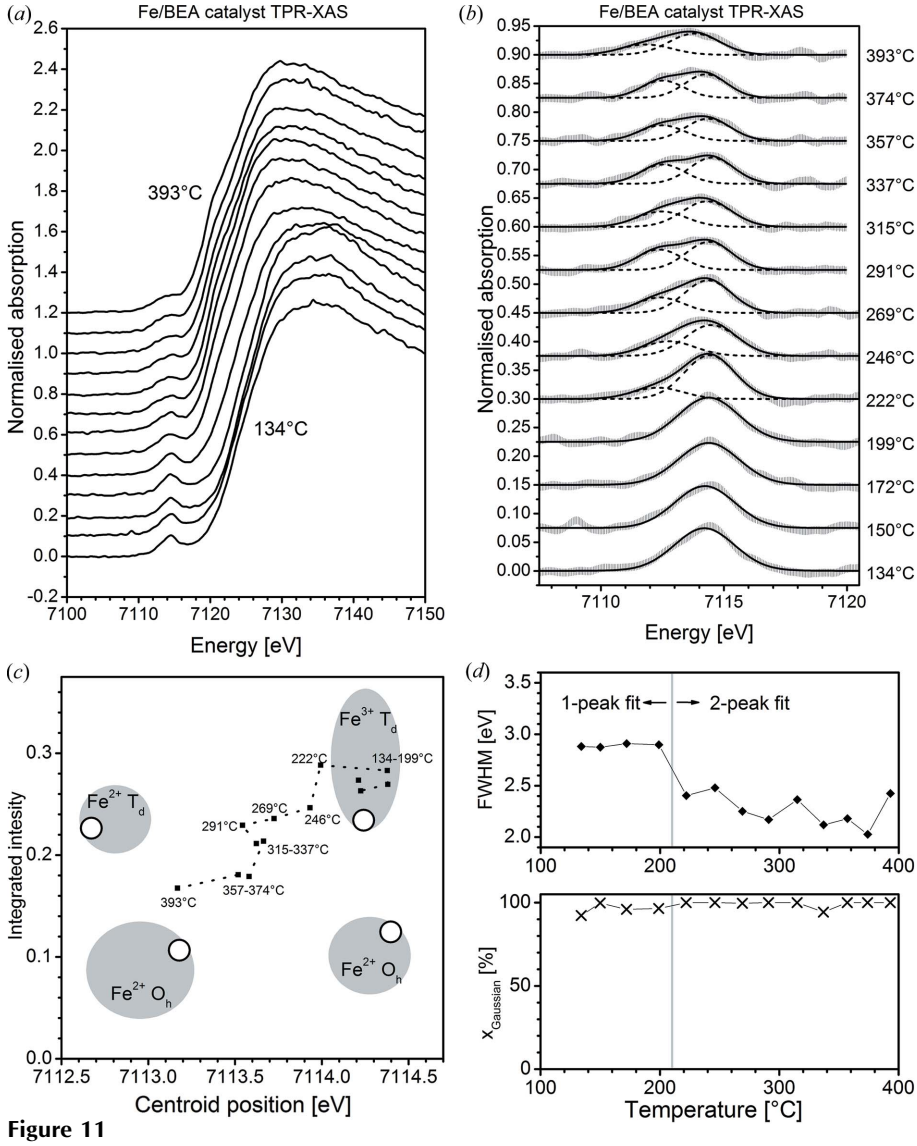

Figure 11
In situ Fe *K*-edge XANES spectra (*a*) and the pre-edge spectra (*b*) of a 0.5% Fe/BEA zeolite catalyst acquired during a TPR experiment with high resolution in fluorescence. The spectra were acquired using continuous energy scans with a period of approximately 5 min per spectrum with energy increments of 0.1 eV [conditions: 20% H_2/He in a quartz capillary micro-reactor, heated up to 400°C (*cf.* Høj *et al.*, 2009)]. The pre-edge spectra in (*b*) were extracted using the inclined arctangent function and fit with one or two pseudo-Voigt peak functions. Variogram (*c*) and evolution with temperature of the peak width (FWHM) and Gaussian fraction ($x_{Gaussian}$) of pseudo-Voigt functions (*d*), analogous to Figs. 10(*a*) and 10(*b*). The vertical grey line separates the FWHM and $x_{Gaussian}$ obtained when fitting the pre-edge spectra with one and two pseudo-Voigt peaks.

inflection points, making the definition of the edge position ambiguous. The edge position is commonly determined using the derivative spectrum, which is potentially sensitive to noise in the data.

4. Conclusion

Fe *K*-pre-edge analysis is an attractive method both in materials science and catalysis for unravelling oxidation state and geometry. Extending the approach by groups like Farges and Wilke, we have shown here that this method can also be a valuable tool to estimate the oxidation state and coordination geometry of Fe centres in catalysts under reaction conditions where typically data are recorded at conventional EXAFS beamlines. The example of an *in situ* pre-edge study revealed that, during reduction of Fe^{3+} to Fe^{2+} in iron-based Al_2O_3 and zeolite catalysts, the local coordination of four to five O atoms stays constant, which is useful information for mechanistic studies of this catalyst for automotive applications. Importantly, the variogram-based analysis of the pre-edge peak allows the local coordination number and the oxidation state to be simultaneously accessed, circumventing the uncertainties due to high noise levels, the temperature-sensitivity of EXAFS as well as related problems with XANES.

Empirical processing of the pre-edge spectra by fitting with robust model functions compensates for the unknown state of iron in the chemical system under investigation, thus maintaining a high degree of objectivity and reproducibility. This is important for studies of heterogeneous catalysts since the structure of the Fe species, mostly in non-crystalline samples, is often unknown. Thus, only the chemical speciation of the Fe sites is important and a chemical similarity of the reference compounds with the compounds under investigation is not a pre-requisite. Similarly, multiple data sets are subject to reliable analysis.

The elegance of using a pre-edge variogram for analysis of Fe lies largely in the fact that the pre-edge peak position is only indicative of the oxidation state, while the intensity is only indicative of the coordination geometry, making it possible to extract these values individually. The number of frequently occurring oxidation states (between Fe^{2+} and Fe^{3+}) and local coordination numbers (between four and six) is low, contributing to a rather accurate analysis. For other first-row transition metals, the position of the *K*-pre-edge peak depends on both the oxidation state and coordination geometry, and often more oxidation states can be expected (*e.g.* in the case of manganese), requiring complementary structural information from XANES and EXAFS.

M. Wilke (GFZ Potsdam) and F. Farges (Museum National d'Histoire Naturelle, Paris) are kindly acknowledged for scientific exchange concerning their earlier studies in the field of pre-edge peak fitting. Furthermore, we thank the following persons who provided us with reference mineral samples: N. E.

Nikol'skaya (FGUP 'VIMS', Russia) for olivine, T. A. Burova (FGUP 'VIMS', Russia) and V. I. Yashina (MGRI-RSGPU, Russia) for siderite, aegirine, ceylonite and bronzite, F. Daliran (KIT, Institute of Applied Geosciences) for staurolite and magnetite and K. Drübbel (KIT, Institute of Applied Geosciences) for sanidine. The XAS beamline at ANKA (KIT) and the ID26 beamline at ESRF are acknowledged for providing beam time. Finally, we thank BMBF (project 'MatAkt') for financial support to build up infrastructure for *in situ* characterization at ANKA.

References

Agostini, G., Lamberti, C., Pellegrini, R., Leofanti, G., Giannici, F., Longo, A. & Groppo, E. (2013). *ACS Catal.* **4**, 187–194.
Atkins, A. J., Bauer, M. & Jacob, C. R. (2013). *Phys. Chem. Chem. Phys.* **15**, 8095–8105.
Bajt, S., Sutton, S. R. & Delaney, J. S. (1994). *Geochim. Cosmochim. Acta*, **58**, 5209–5214.
Bare, S. R. & Ressler, T. (2009). *Adv. Catal.* **52**, 339–465.
Battiston, A. A., Bitter, J. H., de Groot, F. M. F., Overweg, A. R., Stephan, O., van Bokhoven, J. A., Kooyman, P. J., van der Spek, C., Vankó, G. & Koningsberger, D. C. (2003*a*). *J. Catal.* **213**, 251–271.
Battiston, A. A., Bitter, J. H., Heijboer, W. M., de Groot, F. M. F. & Koningsberger, D. C. (2003*b*). *J. Catal.* **215**, 279–293.
Berry, A. J., O'Neill, H. S., Jayasuriya, K. D., Campbell, S. J. & Foran, G. J. (2003). *Am. Mineral.* **88**, 967–977.
Bordiga, S., Groppo, E., Agostini, G., van Bokhoven, J. A. & Lamberti, C. (2013). *Chem. Rev.* **113**, 1736–1850.
Boubnov, A., Carvalho, H. W. P., Doronkin, D. E., Günter, T., Gallo, E., Atkins, A. J., Jacob, C. R. & Grunwaldt, J.-D. (2014). *J. Am. Chem. Soc.* **136**, 13006–13015.
Boubnov, A., Lichtenberg, H., Mangold, S. & Grunwaldt, J.-D. (2013). *J. Phys. Conf. Ser.* **430**, 012054.
Brandenberger, S., Kröcher, O., Tissler, A. & Althoff, R. (2008). *Catal. Rev.* **50**, 492–531.
Caliebe, W. A., Kao, C. C., Hastings, J. B., Taguchi, M., Kotani, A., Uozumi, T. & de Groot, F. M. F. (1998). *Phys. Rev. B*, **58**, 13452–13458.
Cottrell, E., Kelley, K. A., Lanzirotti, A. & Fischer, R. A. (2009). *Chem. Geol.* **268**, 167–179.
Deutschmann, O. & Grunwaldt, J.-D. (2013). *Chem. Ing. Tech.* **85**, 595–617.
Dong, H. H., Xie, M. J., Xu, J., Li, M. F., Peng, L. M., Guo, X. F. & Ding, W. P. (2011). *Chem. Commun.* **47**, 4019–4021.
Doronkin, D. E., Casapu, M., Günter, T., Müller, O., Frahm, R. & Grunwaldt, J.-D. (2014*b*). *J. Phys. Chem. C*, **118**, 10204–10212.
Doronkin, D. E., Fogel, S., Gabrielsson, P., Grunwaldt, J.-D. & Dahl, S. (2014*a*). *Appl. Catal. Environ.* **148–149**, 62–69.
Dräger, G., Frahm, R., Materlik, G. & Brümmer, O. (1988). *Phys. Status Solidi B*, **146**, 287–294.
Englisch, M., Lercher, J. A. & Haller, G. L. (1996). *X-ray Absorption Fine Structure for Catalysts and Surfaces*, edited by Y. Iwasawa, pp. 276–303. Singapore: World Scientific.
Farges, F. (2005). *Phys. Rev. B*, **71**, 155109.
Farges, F., Lefrère, Y., Rossano, S., Berthereau, A., Calas, G. & Brown, G. E. Jr (2004). *J. Non-Cryst. Solids*, **344**, 176–188.
Galoisy, L., Calas, G. & Arrio, M. A. (2001). *Chem. Geol.* **174**, 307–319.
Ginibre, C., Wörner, G. & Kronz, A. (2004). *J. Petrol.* **45**, 2197–2223.
Glatzel, P., Sikora, M. & Fernández-García, M. (2009). *Eur. Phys. J. Spec. Top.* **169**, 207–214.
Groot, F. de, Vankó, G. & Glatzel, P. (2009). *J. Phys. Condens. Matter*, **21**, 104207.
Grunwaldt, J. D. (2009). *J. Phys. Conf. Ser.* **190**, 012151.
Grunwaldt, J.-D., Caravati, M., Hannemann, S. & Baiker, A. (2004). *Phys. Chem. Chem. Phys.* **6**, 3037–3047.
Grunwaldt, J.-D. & Clausen, B. S. (2002). *Top. Catal.* **18**, 37–43.
Grunwaldt, J.-D., Hannemann, S., Göttlicher, J., Mangold, S., Denecke, M. A. & Baiker, A. (2005). *Phys. Scr.* T**115**, 769–772.
Grunwaldt, J.-D., van Vegten, N. & Baiker, A. (2007). *Chem. Commun.* pp. 4635–4637.
Hazen, R. M. & Jeanloz, R. (1984). *Rev. Geophys.* **22**, 37–46.
Heijboer, W. M., Glatzel, P., Sawant, K. R., Lobo, R. F., Bergmann, U., Barrea, R. A., Koningsberger, D. C., Weckhuysen, B. M. & de Groot, F. M. F. (2004). *J. Phys. Chem. B*, **108**, 10002–10011.
Høj, M., Beier, M. J., Grunwaldt, J.-D. & Dahl, S. (2009). *Appl. Catal. Environ.* **93**, 166–176.
Klukowski, D., Balle, P., Geiger, B., Wagloehner, S., Kureti, S., Kimmerle, B., Baiker, A. & Grunwaldt, J.-D. (2009). *Appl. Catal. Environ.* **93**, 185–193.
Liu, F., He, H. & Xie, L. (2013). *ChemCatChem*, **5**, 3760–3769.
Liu, H., Wang, J., Yu, T., Fan, S. & Shen, M. (2014). *Catal. Sci. Technol.* **4**, 1350–1356.
Maier, S. M., Jentys, A., Metwalli, E., Müller-Buschbaum, P. & Lercher, J. A. (2011). *J. Phys. Chem. Lett.* **2**, 950–955.
Mangold, S., Steininger, R., Rolo, T. dos S. & Göttlicher, J. (2013). *J. Phys. Conf. Ser.* **430**, 012130.
Marturano, P., Drozdová, L., Pirngruber, G. D., Kogelbauer, A. & Prins, R. (2001). *Phys. Chem. Chem. Phys.* **3**, 5585–5595.
Meunier, F. C. (2010). *Chem. Soc. Rev.* **39**, 4602–4614.
Newville, M. (2001). *J. Synchrotron Rad.* **8**, 322–324.
Pirngruber, G. D., Grunwaldt, J.-D., Roy, P. K., van Bokhoven, J. A., Safonova, O. & Glatzel, P. (2007). *Catal. Today*, **126**, 127–134.
Pirngruber, G. D., Roy, P. K. & Weiher, N. (2004). *J. Phys. Chem. B*, **108**, 13746–13754.
Quartieri, S., Riccardi, M. P., Messiga, B. & Boscherini, F. (2005). *J. Non-Cryst. Solids*, **351**, 3013–3022.
Ravel, B. & Newville, M. (2005). *J. Synchrotron Rad.* **12**, 537–541.
Roe, A. L., Schneider, D. J., Mayer, R. J., Pyrz, J. W., Widom, J. & Que, L. (1984). *J. Am. Chem. Soc.* **106**, 1676–1681.
Royer, S. & Duprez, D. (2011). *ChemCatChem*, **3**, 24–65.
Schlögl, R. (2003). *Angew. Chem. Int. Ed.* **42**, 2004–2008.
Schmid, R., Wilke, M., Oberhänsli, R., Janssens, K., Falkenberg, G., Franz, L. & Gaab, A. (2003). *Lithos*, **70**, 381–392.
Shelef, M. (1995). *Chem. Rev.* **95**, 209–225.
Simonsen, S. B., Chakraborty, D., Chorkendorff, I. & Dahl, S. (2012). *Appl. Catal. Gen.* **447–448**, 22–31.
Tepluchin, M., Casapu, M., Boubnov, A., Lichtenberg, H., Wang, D., Kureti, S. & Grunwaldt, J.-D. (2014). *ChemCatChem*, **6**, 1763–1773.
Topsøe, H. (2003). *J. Catal.* **216**, 155–164.
Wagloehner, S., Reichert, D., Leon-Sorzano, D., Balle, P., Geiger, B. & Kureti, S. (2008). *J. Catal.* **260**, 305–314.
Waychunas, G., Apted, M. & Brown, G. Jr (1983). *Phys. Chem. Miner.* **10**, 1–9.
Webb, S. M. (2005). *Phys. Scr.* T**115**, 1011.
Weckhuysen, B. M. (2003). *Phys. Chem. Chem. Phys.* **5**, 4351–4360.
Westre, T. E., Kennepohl, P., DeWitt, J. G., Hedman, B., Hodgson, K. O. & Solomon, E. I. (1997). *J. Am. Chem. Soc.* **119**, 6297–6314.
Wilke, M., Farges, F., Petit, P. E., Brown, G. E. & Martin, F. (2001). *Am. Mineral.* **86**, 714–730.
Wilke, M., Hahn, O., Woodland, A. B. & Rickers, K. (2009). *J. Anal. At. Spectrom.* **24**, 1364–1372.
Wilke, M., Partzsch, G. M., Bernhardt, R. & Lattard, D. (2005). *Chem. Geol.* **220**, 143–161.
Yamamoto, T. (2008). *X-ray Spectrom.* **37**, 572–584.